POLITECNICO DI TORINO

Master of science in Electronic engineering

Master degree Thesis

Design of Dual-Band Millimeter-Wave Antenna
for 5G (26-39 GHz)

Academic Advisor:

Prof. Ladislau MATEKOVITS

Author :

El hadj Mohamed TRAORE

Company Tutor :

Philippe RATAJCZAK

April 2021

ABSTRACT

The first generation of wireless mobile telephony appeared in the 1980s. Since then, the mobile phone generation cycle is about 10 years and the 5G is announced commercially for 2020. With the advent of 5G networks, a need to connect most devices and gadgets together and to the internet has become inevitable. Therefore, high performance antennas are needed to meet more and more higher requirements for new systems. Wideband, wide-scanning array have been receiving great attentions for achieving large bandwidth over a wide scan volume.

The aim of this internship is to design an antenna operating in the 26-39 GHz bands of future ultra 5G systems. This document starts with a general introduction of ORANGE. Then it follows with the presentation of the project and its technical existing solutions. The middle part treats the design of a 6-15GHz connected slot array loaded with artificial dielectrics and its transformation into a 26-39 GHZ dual band antenna. The last part deals with the prospects of this project and the general review of the internship.

Acknowledgements

I would like to acknowledge everyone who played a role in my academic accomplishments.

I would like to express my deep gratitude to M. Eric BONNEAU who gave me the golden opportunity to do this exciting thesis internship in such prestigious establishment . I would also like to thank M. Philippe RATAJCZAK for his patient guidance, enthusiastic encouragement, and useful critiques during the development of the ideas in this research work. I want also to thank both of them for their moral support during the lockdown period caused by the corona virus pandemic.

I also thank the whole team for their welcome and collaboration as well as their spirit.

I would like to extend my sincere thanks to my ENSIL-ENSCI and POLITECNICO DI TORINO professors who have offered me support, feedbacks, and suggestions during my double degree cursus.

I would like to express my special thanks to my parents for their support throughout my life. Thank you for your encouragements in many moments of crisis.

To all my friends, thank you for the amazing time we passed together, your friendship makes my life a wonderful experience. I cannot list all of you here, but you are always in my heart.

Table of Contents

List of Figures

List of Tables

1. **Introduction**

As part of my double degree cursus, I completed a six-month internship in the "Technology and Global Innovation" division of ORANGE.

I joined the antenna specialist team, based in Sophia-Antipolis, in charge of specifications, design, optimization, testing and evaluation of antennas that are , will be or could be used by ORANGE, in base stations and mobile network terminals(4G, 5G), Wi-Fi access points, the Internet of Things, Machine-to-Machine type communications, or future applications using millimetre waves (25-260 GHz).

My mission was to design an antenna operating in the 26-39 GHz bands of future very high-speed 5G systems.

With this objective, I first performed a general study of wideband antenna existing solutions afterward I proposed a solution that could match with the requirements. Then I designed a 6-15 GHz connected slot array loaded with artificial dielectric superstrates. I finished with a transformation from the 6-15 GHz prototype to the 26-39 GHz dual band antenna.

2. The Firm

2.1. Company Introduction

ORANGE is one of the world's leading telecommunications operators with sales of 42 billion euros in 2019 and 145,000 employees worldwide at 31 March 2020, including 85,000 employees in France. The Group has a total customer base of 253 million customers worldwide at 31 March 2020, including 208 million mobile customers and 21 million fixed broadband customers. The Group is present in 26 countries. ORANGE is also a leading provider of global IT and telecommunication services to multinational companies, under the brand Orange Business Services. In December 2019, the Group presented its new "Engage 2025" strategic plan, which, guided by social and environmental accountability, aims to reinvent its operator model. While accelerating in growth areas and placing data and AI at the heart of its innovation model, the Group will be an attractive and responsible employer, adapted to emerging professions.

2.2. Activities

2.2.1. Networks

Our lives have been transformed as a result of network access. Most people around the world have mobile coverage and half are now online. This revolution is made possible by high-tech telecommunications networks, whether undersea or up in space, that help us to exchange ever more information, faster and more easily. Managing them has always been Orange's core business.

Orange is one of the main global telecommunications network operators offering connectivity services to individuals, business, and other operators. To manage all its thousands of technical sites and data centres, millions of kilometres of optical fiber and copper cables, hundreds of thousands of items of equipment, tens of thousands of antennas are employed.

Networks are the cornerstone of Orange's innovation and a core pillar of its strategy. Around 34,000 Orange employees around the world are dedicated to their design, deployment, supervision, maintenance, and modernisation.

Orange is today the leader in very-high speed broadband with more than 39.5 million homes connectable to optical fiber around the world at the end of 2019, an increase of 21.5% in one year.

- **Mobile network**

By being the #1 mobile network in France for the 9th time in a row according to the ARCEP report of October 2019, Orange provides the best quality of mobile services for streaming video, calls , SMS, and mobile Internet.

- **Fiber coverage and Orange's internet**

Orange is the operator that provided the highest performance fixed Internet access to its subscribers in 2019.

Orange is the first fixed Internet network according to the nPerf barometer, specialist in the evaluation of telecom connections. This result, Orange owes it to its sustained efforts and the investments that are more than 1 billion euros each year in the deployment of Fiber, in order to offer Very High-Speed Internet to all its customers. More than 18 million catches already eligible for Fibre at the end of 2019, an increase of more than 36% in 1 year. With its ambitions to offer THD to every household by 2023, France will be one of the best equipped countries in the world.
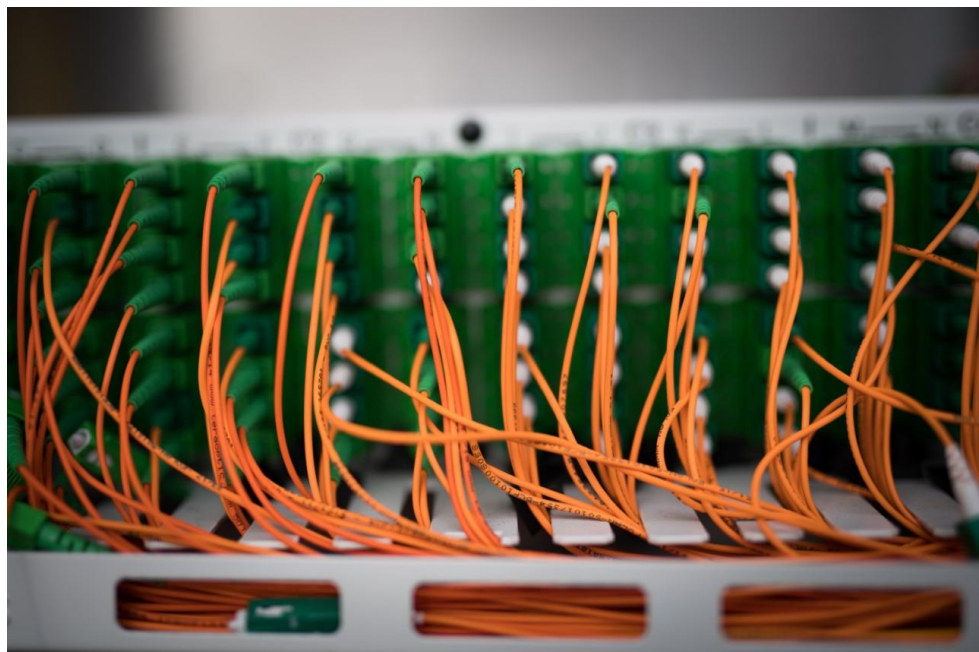
Figure 1: close-up of optical fiber cables

2.2.2. Orange Content

Offer an attractive content proposition today while creating great entertainment for tomorrow is the aim targeted by Orange Content. Orange content was launched in 2017, reaffirming the Group's ambition and strategy first implemented in 2008. The goal is to offer its customers a unique digital entertainment experience, which is diverse, riche and available at all times, whether at home or on the move and via all networks and platforms: TV, PC, mobile and tablet.

Very high-speed connectivity has enabled customers to access a host of new entertainment services. For more than a decade, Orange has been investing in a diverse catalogue of top quality audiovisual and cultural content. Orange content leads the overall strategy of Orange and relies on developing partnerships with rights holders and service providers.

Orange content brings together several resources and assets dedicated to the following activities :

- **Orange Studio** : a subsidiary focused on coproducing films and acquiring titles
- **OCS**: the premium service for fans of films and series, available via linear broadcasting or on demand
- **Orange Prestations TV** : Orange's broadcasting platform

Orange content also looks after other content-related activities (including games, music, culture, infotainment, virtual reality) as well as the French and international content acquisition activities for all services edited by Orange and multi-territory negotiations for third parties.

Figure 2: Content offers in Europe, in Africa and the Middle East

2.2.3. Enterprise Services

Orange's subsidiaries support companies active in various sector. Digitalization has created new needs within companies : collaborative working methods, optimized performance of information systems and 360 ° customer relations. Orange's consultants and experts support the transformation of technological and human processes by providing services such as organizational analysis, formalization of needs, functional specifications, or performance measurement.

Orange Business Services in numbers :

- More than 160 countries and territories covered
- 21,500 employees
- 15 research and innovation laboratories
- 227 million customers

2.2.4. Orange Financial services

The needs for networks, the cloud, data, and data security has assisted digital players in entering the financial sector. They are the originators of a profound transformation in the model for this sector, to the benefit of users. This change invites us to think natively digital and to prioritize mobile. Orange is revolutionizing financial services with its two financial services Orange Bank and Orange Money.

- **Orange Bank** : a complete banking package offering its customers innovative banking services which are designed for mobiles and without any income criteria.
- **Orange Money**: since its launch in Côte d'Ivoire, 45 million customers in 18 countries rely on Orange Money to access simple and secure financial services that make life easier every day. Orange Money is now a major growth driver for Orange. As an essential service in Africa, it also offers future market potential in Europe.

45million

customers (end of 2019)

€425 million

revenue in 2019.

€43 million

in transactions.

1 billion

transactions in one
week.

220,000 points

of sale.
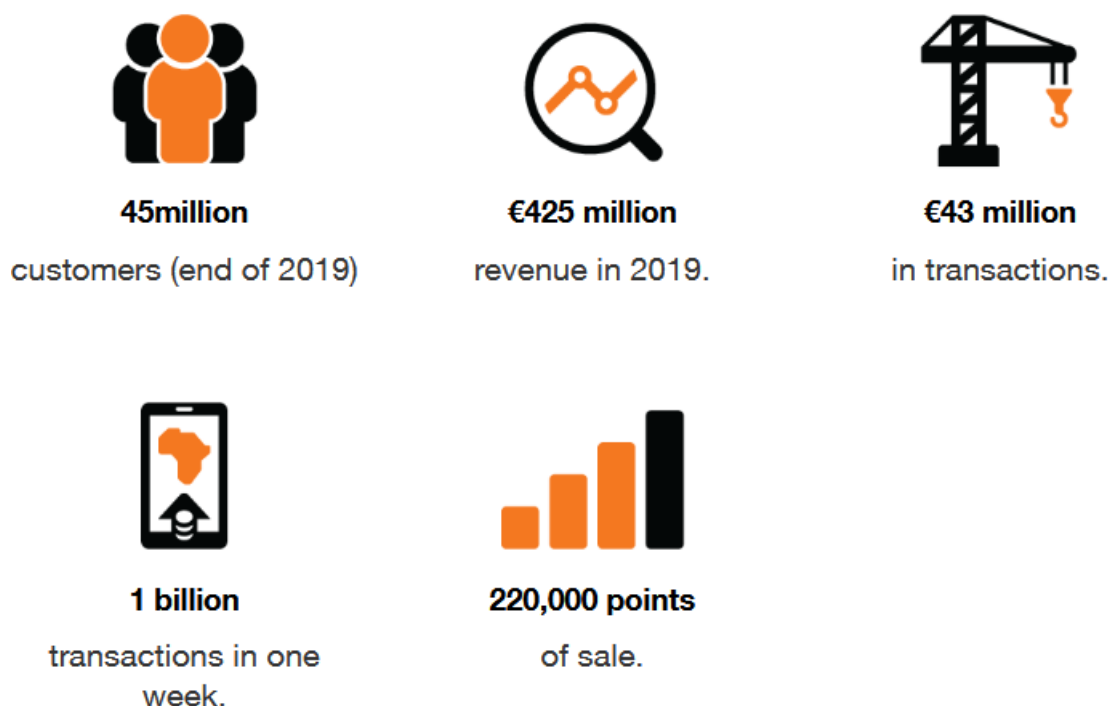
Figure 3: Key figures of Orange Money

- **Orange Bank Africa :** on 23 July 2020, Orange and NSIA launched Orange
  Bank Africa to provide greater access to financial services and improve the
  financial inclusion of people living in West Africa. It will address the needs
  of a large part of the population, often excluded from the world of
  conventional banking, allowing them to borrow and save small amounts
  that are nonetheless essential for their everyday lives.

2.3. Technology and Global Innovation division

In a context of rapid changes in customer uses and expectations, technological breakthroughs,
increasing competition from new players and new business models, the mission of TGI (technology
and Global Innovation) is to prepare Orange's future with countries and our ecosystems by building
differentiating competitive advantages. This mission is based on 4 axes: to support the Group's
technological and data strategy, to drive major innovation, to support countries in their innovation
process, and to build and operate shared solutions.

2.3.1. The staff

Figure 4: Organization chart of TGI

2.3.2. Team Antenna

Within the IMT division (Innovation, Marketing, Technologies), are Orange Labs which are the Research and Development Division of the Orange Group. They are subdivided in OLN poles that make up Orange's global innovation network.

The OLN division defines and manages the Group's strategy in the field of network design and operation. It supports countries in their operational implementation.

The OLN teams ensure that the Group's strategy is considered in the development of telecom standards and norms and in the products and services of the manufacturers chosen by the Group.

Finally, OLN supplies the Group with network innovations to fuel the engine of growth

The RNM (Radio access Networks and Microwaves) department is in charge of infrastructure architecture, technologies, equipment, deployment and optimization methods, operation

and associated tooms for radio access networks, over-the-air transport solutions as well as connectivity access network solutions.

The RIO (Radio Innovation) department within Orange Labs is in charge of carrying out studies on radio access technologies (Wi-Fi, LTE (4G),5G)and conducting outdoor Wi-Fi and antennal performance evaluations.

The ANT (Antenna) department is in charge of antenna design and measurement for Orange projects. It is also called upon for the measurement of antennas from outside companies or laboratories.

3. Presentation of the Project

3.1. Topics

3.1.1.　　5G

5G is the new generation of mobile telecommunications, even more efficient than previous ones. It allows mobile networks to make enormous progress in terms of throughput, responsiveness, and adaptability to usage. It responds to the needs and challenges of tomorrow, including by radically transforming our modes of connection into mobility. 5G uses the same radio waves as current technologies and therefore part of the current recommendations and regulations. 5G also supports the development of applications that require increased responsiveness such as gaming or enhanced industrial maintenance.
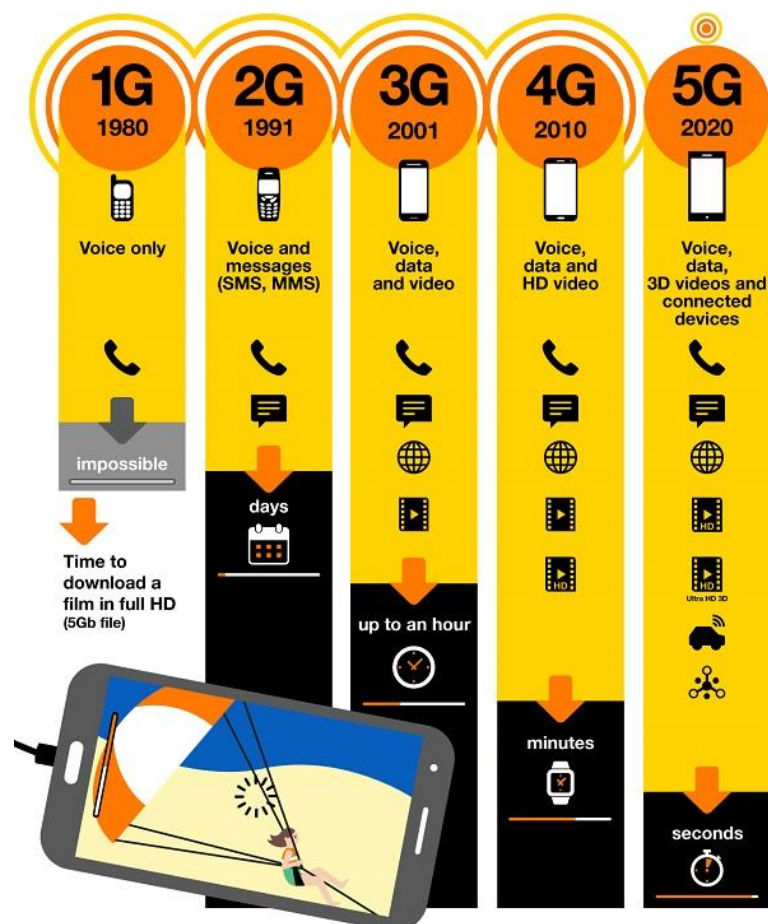
Figure 5: Evolution of mobile network uses

3.1.2. Frequencies

The implementation of 5G depends on several technical solutions, which will be put in place gradually. 5G mobile antennas will eventually use 3 frequency bands.

The 700 MHz band, already used by some operators for 4G, has the benefit of enabling a good penetration inside buildings and good coverage with speeds comparable to those of monoband 4G.

The 3.6 GHz (3.4- 3.8 GHz) bands helps to significantly ramp up speeds despite lower penetration inside buildings and lower reach than the 700 MHz band.

The 26 GHz (24.5-27.5 GHz) band is the highest frequency used in mobile technology and it can deliver very high speeds, comparable to those of FTTH (Fiber). On the other hand, its ability to penetrate buildings is very low as it cannot go through obstacles and its reach is limited to a few hundred metres.

The first 5G deployments are taking place mainly in the 3.5 GHz frequency bandwidth, which is a bandwidth very close to current mobile networks (3G/4G and Wi-Fi) in terms of coverage.

With the combination of these 3 bands, speeds could go as high as a theoretical maximum 10 Gbps.

3.1.3. Antennas

3.1.3.1. Definition

In radio engineering, an antenna is the interface between radio waves propagating through space and electric currents moving in metal conductors, used with a transmitter or receiver. In transmission, a radio transmitter supplies an electric current to the antenna's terminal, and the antenna radiates the energy from the current as electromagnetic waves. In reception, an antenna intercepts some of the power of a radio wave in order to produce electric current at its terminals, that is applied to a receiver to be amplified.

Since all wireless systems are based on the radiation and/ or reception of electromagnetic waves, knowledge of antennas is a key competence in communication system design. Understanding the limitations imposed by electromagnetic interference is a necessary competence in communication systems and also in any electronic hardware or electronic modern integrated circuits design.

3.1.3.2.   5G antennas

The main difference between 5G and existing networks will be the use of *MIMO smart antennas*, each made up of a large number of miniaturized antennas which make it possible to reach speeds and transmission capacity that are inaccessible today in 4G.

The massive **MIMO antenna** acts like a directional beam, the signal is pointed in a precise direction instead of transmitting in all directions. The massive MIMO antenna thus reduces energy losses by transmitting radio waves only where these are useful. It makes it possible to direct the radio signal to users and devices whenever necessary, rather than transmitting all the time and everywhere. This characteristic enables antennas to switch to standby when they are not activated, offering better energy consumption management. Any superfluous waves around users are therefore considerably reduced or even eliminated.

Figure 6: 4G antenna vs 5G antenna

Furthermore, in certain network cells, small additional antennas can be installed to provide additional coverage and capacity for certain "blind" zones. These small additional antennas may be located on street furniture or inside buildings.

11

3.2. Goals

The overall objective is to be able to integrate into a team, to understand the technology, and to be able to innovate on this technology. Another interesting point is to be able to take responsibility by developing a project independently. As part of a team at the forefront of research, I had the opportunity to work and participate in a real project. The purpose of my internship is to conduct and design an antenna operating in the 26-39 GHz bands. Therefore, I had to :

-Analyse the different technical solutions to achieve the technical specifications (gain, S11, efficiency, etc.) for this type of antenna.

-Design from the selected technical solution, the antenna meeting the specifications in order to have it manufactured.

-Participate in the prototype testing campaign.

Unfortunately, because of the health crisis related to the corona virus, I was only able to meet the team ANT and my supervisor 3 months after the start of my internship. Then, I had the opportunity to visit the anechoic chamber used at Orange lab Sophia Antipolis.

Nevertheless, several steps of the project have been completed during these 3 months of lockdown. I started by the the literature review to find an antenna that could satisfy the requirements of the project. After analysing the different existing solutions, I proposed a 6-15GHz wideband slot connected array loaded with artificial dielectric superstrates. Designed perfectly, this antenna could meet the 26-39GHz dual band antenna requirements by applying a transformation on the dimensions of the 6-15GHz prototype. The final antenna obtained should have good performances in terms of **matching** (VSWR, return loss S11),**directivity, gain** and **efficiency** in the 26-39GHz bands.

4. **Technical Solutions**

Before detailing the different wideband antenna solutions, we should mention that several solutions of structure are possible for the design of our antenna:

-Dual-band

-Nested mono-bands

-Wideband

The main problem arises when we want to perform high angle steering for the two bands (26GHz and 39GHz):

-Starting from the conventional design(dual band), the size of the array cell is fixed by the low frequency but the angle of steering at the high frequency without grating lobe is reduced.

-We can try to design two nested independent structures (different sizes of basic elements) to keep the same coverage without grating lobes but the design becomes complex.

-Work on a wideband structure :

- o   If the size is fixed by the low frequency, we face the same problem as for a dual band structure
- o   If the size is set by the high frequency, no more grating lobes issue but we have an over-sampling problem for the low frequencies.

The last solution is interesting but since the structure of this type of antenna seems to be complex, It is necessary to work on an "approached" analysis that facilitates the pre-design before validating the structure by a global analysis under a simulation software (CST, HFSS…).

4.1. Typical wideband antenna solutions

Wideband, wide scanning arrays have been receiving great attention in the last few decades for both commercial and military applications, such as satellite communications, radio astronomy and broadband radars. Several solutions have been proposed to realize wideband wide scanning arrays. These includes stacked patches, tapered slot antennas and tightly coupled dipole arrays. These examples have attained wideband properties.

13

4.1.1. Stacked Patches

4.1.1.1. Microstrip patch antenna

➤ A **patch antenna** is a type of radio antenna with a low profile, which can be mounted on a flat surface. It consists of area of metallization supported above a ground plane by a thin dielectric substrate and fed against the ground at an appropriate location. The patch shape can in principle be arbitrary. In practice, the rectangle, the circle, the equitriangle and the annular-ring are common shapes. The basic structure of a microstrip patch antenna is shown in figure 7.
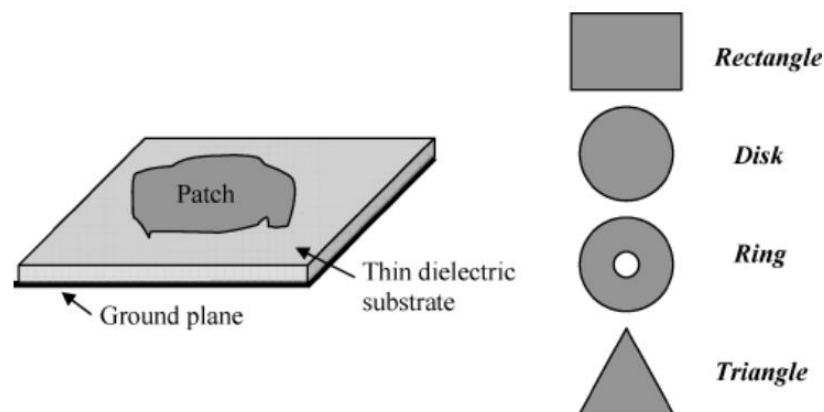
Figure 7: Basic structure of a microstrip patch antenna

➤ **Advantages of Microstrip patch antennas** : planar, which can also made conformal to a shaped surface, low profile, low radar cross-section, rugged, can be produced by printed circuit technology, can be integrated with circuit elements, can be designed for dual polarization operations, can be designed for dual or multi-frequency operations.

➤ **Disadvantages of microstrip patch antennas** : narrow impedance bandwidth (typically less than 5%), due to the small separation between the radiating patch and its ground plane, the microstrip antenna can handle relatively low RF power, microstrip arrays generally have larger ohmic loss than arrays of other types of antenna of equivalent size aperture.

4.1.1.2. Stacked configuration

As mentioned previously, microstrip patch antenna can be designed for dual or multi-frequency operation and even if the microstrip antenna has narrow bandwidth in its basic form, various bandwidth widening techniques have been developed.

Thus, stacked patches are one of the most typical antenna solutions used in wideband, wide scanning arrays. They have been shown to achieve about an octave bandwidth for a linearly polarized array. However, the maximum possible bandwidth achievable with this solution is limited by the resonant nature of the radiators.
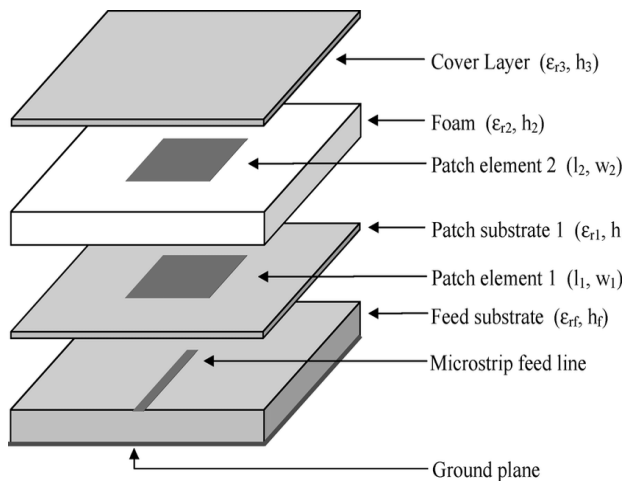
Figure 8: A stacked proximity coupled patch antenna structure
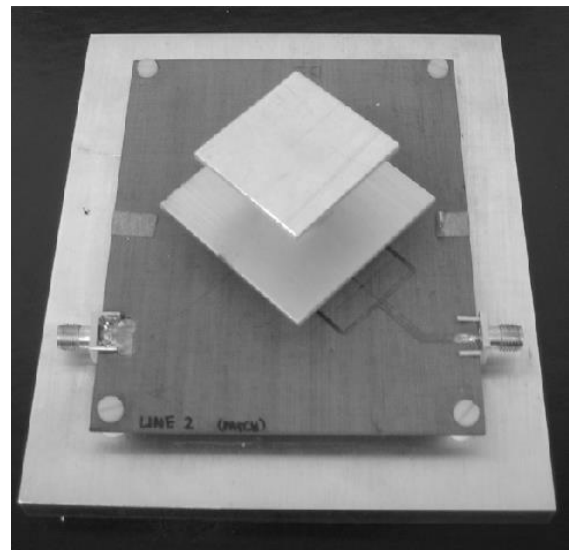
Figure 9: A stacked patch antenna prototype

4.1.2. Tapered Slot antennas

The radiation mechanism of a tapered slot antenna (TSA) is based on traveling propagation wave along the tapered slot, which results in an end fire antenna. TSA belong to the class of traveling wave antenna. TSA exhibits some advantages such as wideband, wide scanning high gain and low cross polarization. Despite the good performances in terms of impedance matching, the large bandwidth comes often at the cost of degraded performances in terms of polarization purity because of the vertical components of the radiating currents along the flared edges.

Figure 10: A manufactured Vivaldi antenna
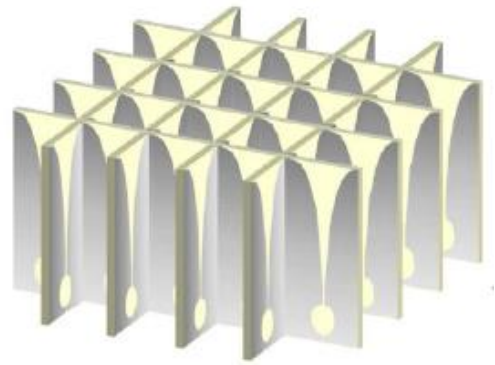
Figure 11: Egg-crate configuration of Vivaldi antenna

4.1.3. Connected arrays

Connected arrays consist of arrays of either slots or dipoles which are electrically connected. They have the advantage of being broadband and, at the same time, they can achieve low cross-polarization levels. Unlike Tapered slot antennas, connected array are based on planar radiating currents with no vertical components, which can guarantee better polarization purity. Although, this is true in principle, practically the feeding network of connected arrays must be designed carefully to maintain undesired radiation from the feed lines as low as possible in all scanning conditions.
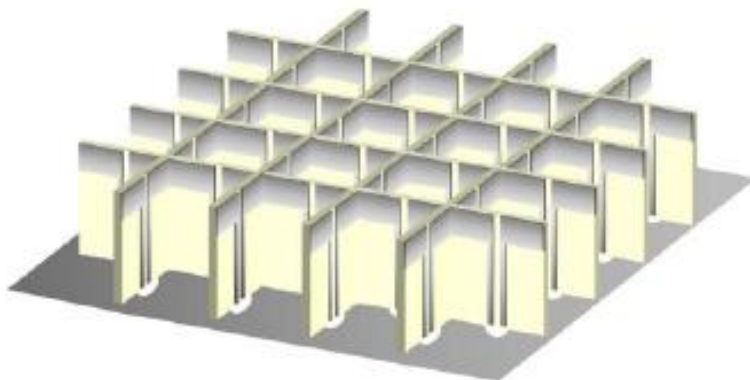
Figure 12: Typical egg-crate configuration for wideband connected dipole array

16

4.2. Wide Scan Planar Array of connected slots loaded with ADLs Superstrates

Unlike resonant antennas, which support sinusoidal and strongly frequency-dependent current distributions, connected arrays are characterized by currents that are weakly frequency dependent, due to the electrical connection between adjacent antenna elements. In practice, the bandwidth of a connected array is limited by the presence of a backing reflector which is required to ensure unidirectional radiation.

In the solution proposed in this project, we combine connected array of slot with artificial dielectric layers (ADLs). Since this configuration is complex, we are going to first define what is an artificial dielectric and secondly, we will describe an analytical tool which helps us to perform the pre-design.

4.2.1.   Artificial dielectric

Artificial dielectrics (ADs) were introduced in the late 1940s by Kock, who proposed a low loss and light weight alternative to real dielectrics for realizing lens antennas. An AD consists of periodic metallic structures embedded in a host material in order to increase its equivalent relative permittivity. These slabs are demonstrated to support much less surface waves than regular slabs of equivalent permittivity. ADs have been extensively studied and used for decades for radar development.

Moreover, artificial dielectric layers (ADLs) can be realized by multiple layers of patches, with dimensions that are small compared to the wavelength as depicted on figure 13 below:
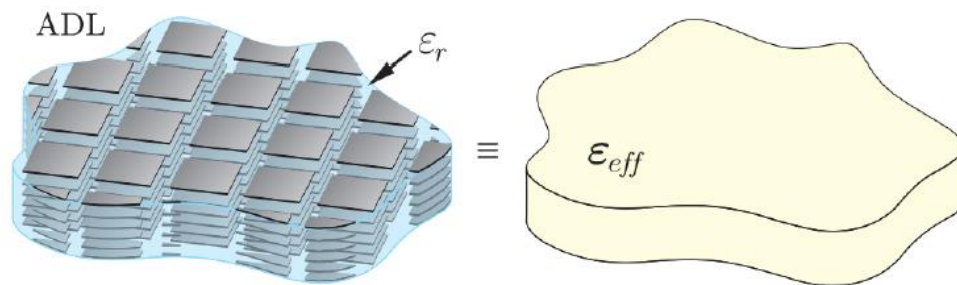
Figure 13: ADL structure and equivalent anisotropic medium

4.2.2. Analysis tool

Because of its complexity, the simulation of the unit cell of the connected array of slots with ADLs would not be a simple or fast process. The entire stack and the electrically small geometrical features would require very fine mesh. In addition, a high number of such simulations are needed to optimize the total structure, rendering the design impractical. For these reasons, a spectral method has been developed to estimate the performance of the connected arrays of slots loaded with ADLs.
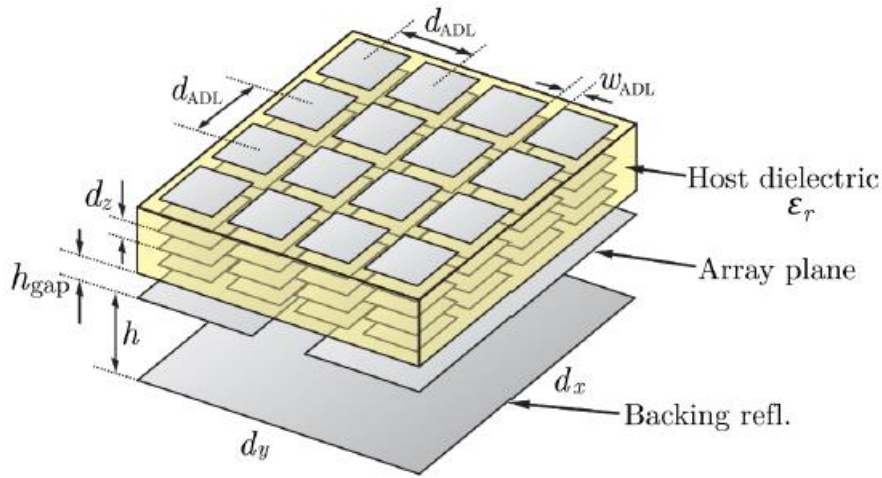
Figure 14: Unit cell of the array loaded with one ADL

4.2.2.1. Closed-Form Analysis of Artificial Dielectric Layers

Properties of a Single Layer Under Plane-Wave Incidence

The scattering from a single layer of periodic square patches has been treated in the literature. Some of these methods provide analytical formulas for the equivalent reactance of the layer under generic plane-wave incidence. However, they do not give a description of the typical properties of these structures, such as transverse electric (TE) and transverse magnetic (TM) modal decoupling and the azimuthal independence of the equivalent layer impedance.

Differently from the previous works, the method described here allows to derive not only a simple analytical formula for the equivalent layer reactance, but also a closed-form expression for the magnetic current distribution on the array plane.

18

Let us consider an infinite doubly-periodic array of patches in free space(figure) :
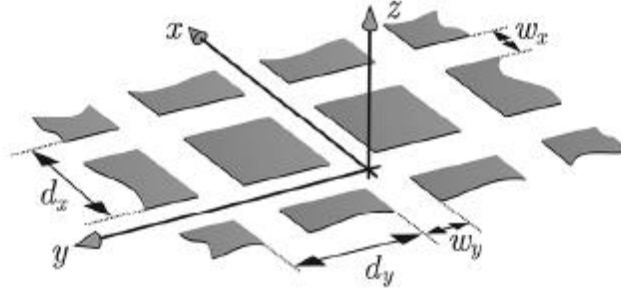
Figure 15: Single layer of crossing slots with geometrical parameters
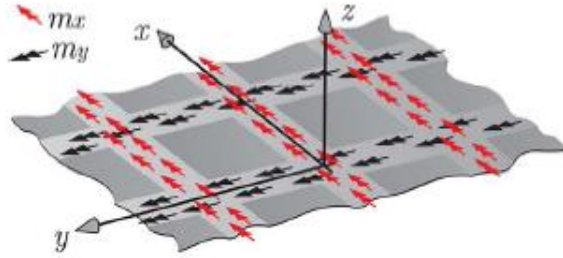
Figure 16: Equivalent magnetic current densities on the slot aperture

We assume that the slots are electrically narrow. The periods along *x* and *y* are indicated by d_x and d_y, respectively w_x and w_y represent the width of the slots oriented along *x* and *y*. From the equivalent principle, magnetic current densities are introduced above and below an infinitely thin metallic layer covering the slot aperture (see figure 16). These equal and opposite currents ensure the continuity of the tangential electric field on the slot aperture. The discontinuity of the magnetic field at the slot plane is expressed in terms of the equivalent current density in convolution integral form :

$$\mathbf{m}(\boldsymbol{\rho}) * \mathbf{g}(\boldsymbol{\rho}) = \int_{-\infty}^{\infty} \int_{-\infty}^{\infty} \mathrm{g}(\boldsymbol{\rho} - \boldsymbol{\rho}'). \mathbf{m}(\boldsymbol{\rho}') \mathrm{d}\boldsymbol{\rho}' = \mathbf{h}_i(\boldsymbol{\rho}) \quad (1)$$

with $\boldsymbol{\rho} \equiv (x, y)$ and $\boldsymbol{\rho}' \equiv (x', y')$, g is the dyadic Green's function related to the Green's function g_{fs} by the condition $g=4g_{fs}$ and g_{fs} represents the magnetic field radiated by an elementary magnetic dipole in free space. A factor 2 comes from the image theorem since the magnetic currents radiate in presence of a perfect electric conductor (PEC). The other factor 2 derives from the fact that the magnetic current

densities above and below the slot aperture must be equal and opposite to satisfy the boundary conditions. $\mathbf{h}_i$ is the incident field in absence of magnetic current but in presence of the ground plane. Then, we have $\mathbf{h}_i = (1 + \Gamma)\mathbf{h}_{dir} = 2\mathbf{h}_{dir}$ since $\Gamma = 1$ the reflection coefficient at the metal, i.e. all the power is reflected at the metal. We then obtain our second equation :

$$\mathbf{m}(\boldsymbol{\rho}) * \mathbf{g}(\boldsymbol{\rho}) = 2\mathbf{h}_{dir} \quad (2)$$

Our structure is illuminated by an arbitrary plane-wave associated with a direct magnetic field $\mathbf{h}dir$, the tangential components of $\mathbf{h}dir$ are generally a superposition of TE and TM modes and expressed as :

$$\mathbf{h}_{dir}(\rho, z) = I_{TE}^+ \mathbf{h}_{TE}(\rho, z) + I_{TM}^+ \mathbf{h}_{TM}(\rho, z) \quad (3)$$

I_{TE}^+ and I_{TM}^+ are the complex weights of the plane-wave components, thus the magnetic field mode functions are given by :

$$\mathbf{h}_{TE}(\rho, z) = \frac{1}{\sqrt{d_x d_y}} \, \hat{\mathbf{k}}_\rho e^{-j\mathbf{k}_\rho \cdot \boldsymbol{\rho}} e^{-jk_{z0}|z|} \quad (4)$$

$$\mathbf{h}_{TM}(\rho, z) = \frac{1}{\sqrt{d_x d_y}} \, \hat{\alpha} e^{-j\mathbf{k}_\rho \cdot \boldsymbol{\rho}} e^{-jk_{z0}|z|} \quad (5)$$

Θ and φ being the elevation and azimuth angles of incidence, the propagation constant respectively along x, y and z given by : $k_{x0} = k_{\rho 0}\cos(\varphi), k_{y0} = k_{\rho 0}\sin(\varphi)$, $k_{z0} = k_0\cos(\theta)$, where k_0 is the free-space wavenumber and $k_{\rho 0} = k_0\sin(\theta)$. The vector $\boldsymbol{k}_\rho$ in the exponential is : $\boldsymbol{k}_\rho = k_{x0}\hat{\mathbf{x}} + k_{y0}\hat{\mathbf{y}}$ and the expressions of the unit vectors of TE and TM components are defined by :

$$\widehat{\mathbf{k}_\rho} = \boldsymbol{cos}(\varphi)\,\hat{\mathbf{x}} + \boldsymbol{sin}(\varphi)\,\hat{\mathbf{y}} = \frac{k_{x0}}{k_{\rho 0}}\,\hat{\mathbf{x}} + \frac{k_{y0}}{k_{\rho 0}}\,\hat{\mathbf{y}} \quad (6)$$

$$\hat{\boldsymbol{\alpha}} = -\boldsymbol{sin}(\varphi)\,\hat{\mathbf{x}} + \boldsymbol{cos}(\varphi)\,\hat{\mathbf{y}} = \frac{k_{y0}}{k_{\rho 0}}\,\hat{\mathbf{x}} + \frac{k_{x0}}{k_{\rho 0}}\,\hat{\mathbf{y}} \quad (7)$$

In order to find a closed-form solution to the equation (2), the unknown magnetic current is expanded into three basis functions defined over the entire unit cell :

$$\mathbf{m}(\boldsymbol{\rho}) = \alpha_{TE}\mathbf{m}_{TE}(\boldsymbol{\rho}) + \alpha_{TM}\mathbf{m}_{TM}(\boldsymbol{\rho}) + \alpha_d\mathbf{m}_d(\boldsymbol{\rho}) \quad (8)$$

α_{TE}, α_{TM} and α_d have to be determined, $\mathbf{m}_{TE}$ and $\mathbf{m}_{TM}$ are the magnetic current enforced by the incident plane-wave on the slots if we neglect the effect of the junctions between crossing slots. $\mathbf{m}_d$ describes the field distribution at the crossing , i.e. considering the effects of the junction between crossing slots. $\mathbf{m}_{TE}$, $\mathbf{m}_{TM}$ and $\mathbf{m}_d$ must verify Kirchhoff's law individually at the crossing and since the first two already satisfy this condition, an appropriate choice for the last one would be the one depicted on figure 17 where the overall magnetic current entering the junction is equal to zero.
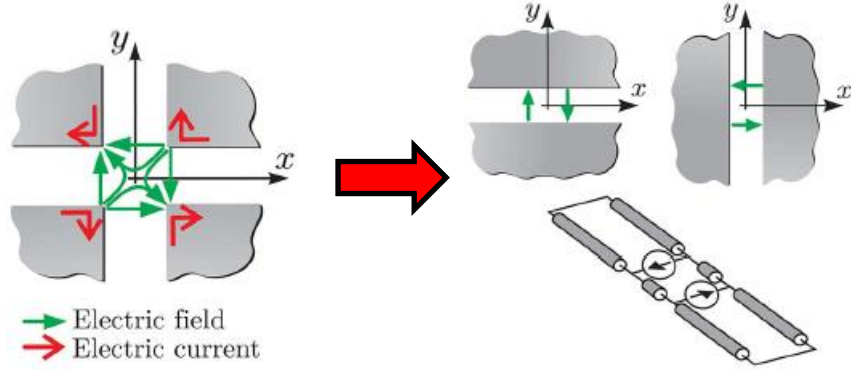
Figure 17 : Electric field and electric current distribution at the junction
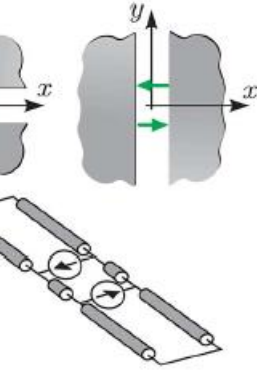
Figure 18: Doublet excitations representing the crossings of orthogonal slots and equivalent line model

The electric field distribution is associated with two equivalent doublet excitations (see fig. 18). The doublet the set of two δ-currents equal and opposite and spaced by a distance equal to the width of the slots.

Solution : By replacing (8) into (2) and applying a Galerkin projection, we obtain a linear system of 3 equations :
$$\begin{cases} \alpha_{TE}Y_{TE,TE} + \alpha_{TM}Y_{TE,TM} + \alpha_d Y_{TE,d} = i_{TE} \\ \alpha_{TE}Y_{TM,TE} + \alpha_{TM}Y_{TM,TM} + \alpha_d Y_{TM,d} = i_{TM} \\ \alpha_{TE}Y_{d,TE} + \alpha_{TM}Y_{d,TM} + \alpha_d Y_{d,d} = i_d \end{cases} \quad (9)$$

Decoupling properties of the structure : this system can be solved for a generic plan-wave incidence by inverting the 3x3 admittance matrix to find the unknown weights. However, for visible plan-wave source and very well sampled array structures, we can assume $i_d \approx 0$, i.e. the current at the junction is null . Therefore, we easily find the expression of α_d from the third equation of (9), substituting it in the first two equations, we obtain the following reduced system:

$$Y_{red} \cdot \begin{bmatrix} \alpha_{TE} \\ \alpha_{TM} \end{bmatrix} = \begin{bmatrix} i_{TE} \\ i_{TM} \end{bmatrix} \qquad (10)$$

Where $Y_{red} = \begin{bmatrix} Y_{TE,TE} - \dfrac{Y_{TE,d} Y_{TE,d}}{Y_{d,d}} & Y_{TE,TM} - \dfrac{Y_{TM,d} Y_{TE,d}}{Y_{d,d}} \\ Y_{TE,TM} - \dfrac{Y_{TM,d} Y_{TE,d}}{Y_{d,d}} & Y_{TM,TM} - \dfrac{Y_{TM,d} Y_{TM,d}}{Y_{d,d}} \end{bmatrix} \quad (11)$

All the admittance elements are calculated in closed form in the spectral domain and then replaced in (11). Y_{red} is therefore written as the sum of 3 terms :

$$Y_{red} = Y_{TL} + Y_{layer} + Y_{cou} \qquad (12)$$

Where Y_{TL} is the admittance of the transmission line, Y_{layer} is the admittance of the ADL layer and Y_{cou} is the coupling admittance and they are defined as :
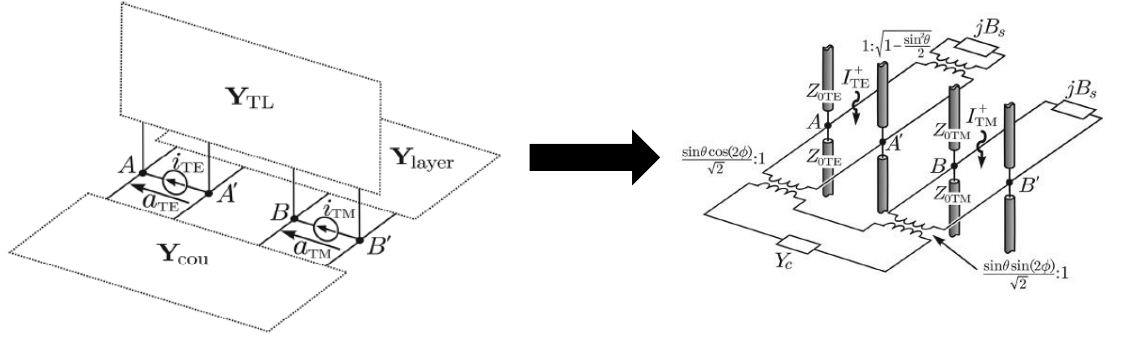
Figure 19: Equivalent circuit representation of Y_{red}

$$Y_{TL} = - \begin{bmatrix} \dfrac{2}{Z_{0TE}} & 0 \\ 0 & \dfrac{2}{Z_{0TM}} \end{bmatrix} \qquad (13)$$

$$Y_{layer} = - \begin{bmatrix} jB_s(1 - \dfrac{sin^2(\theta)}{2}) & 0 \\ 0 & jB_s \end{bmatrix} \qquad (14)$$

$$Y_{cou} = \begin{bmatrix} Y_c \dfrac{sin^2(\theta) cos^2(2\varphi)}{2} & -Y_c \dfrac{sin^2(\theta) \, sin(2\varphi) \, cos(2\varphi)}{2} \\ -Y_c \dfrac{sin^2(\theta) \, sin(2\varphi) \, cos(2\varphi)}{2} & Y_c \dfrac{sin^2(\theta) sin^2(2\varphi)}{2} \end{bmatrix} \quad (15)$$

Z_{0TE} and Z_{0TM} are respectively the wave impedance of the TE and TM modes, B_s is the slot self-susceptance and Y_c is the coupling admittance term.

$$Z_{0TE} = \frac{\xi_0 k_0}{k_{z0}} \qquad\qquad Z_{0TM} = \frac{\xi_0 k_{z0}}{k_0}$$

Therefore, the slot susceptance B_s is defined as the sum of higher Floquet modes :

$$B_s = \frac{2k_0}{\xi_0} \sum_{m_y \neq 0} \frac{|sinc(k_{ym}w_x/2)|^2}{|k_{ym}|} \qquad (16)$$

With $k_{ym} \approx (2\pi m_y)/(d_y)$.

Finally, the equivalent reactances of the layer for TE and TM incidence are given by :

$$Y_{layer,TM} = \frac{-j}{B_s} \qquad\qquad Y_{layer,TE} = \frac{-j}{B_s\left(1 - \frac{sin^2(\theta)}{2}\right)} \qquad (17)$$

impedance $\longrightarrow$ Z=R+jX   admittance $\longrightarrow$ Y=G+jB

resistance   reactance   conductance   susceptance
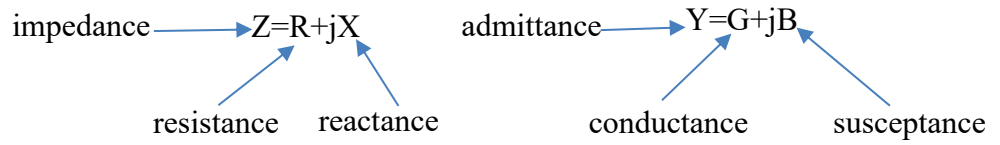
(16) and (17) have been written in MATLAB (appendix A) in order to plot the equivalent reactance of the isolated layer. The result obtained is depicted on fig.20.
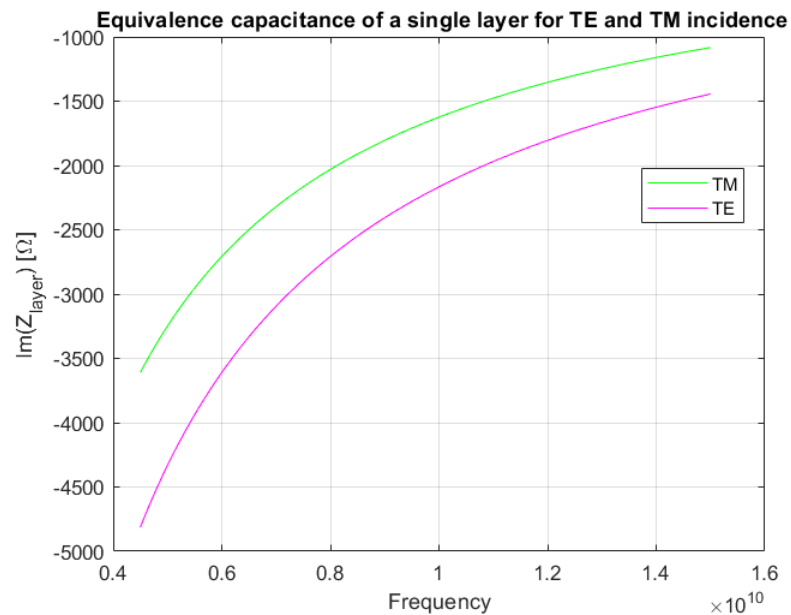
Figure 20: Equivalent capacitance of a single layer for TE and TM incidence from $\theta_i = 45°$ with $w_y = w_x = 0.02\lambda$ and $d_y = d_x = 0.15\lambda$ where λ is the wavelength at the frequency $f_0 = 15GHz$

Extension to Multiple Layers and Arbitrary Illumination

In realistic designs, ADLs are composed by several layers stacked together with very small electrical interlayer distance which significantly changes the reactance that the layers would have in isolation. Therefore, in this part, we generalize the formulation presented in the previous part to account for the coupling between the layers.

Let us consider an infinite number of layers periodically spaced along z axis with interlayer distance d_z as depicted in fig. 21 below.
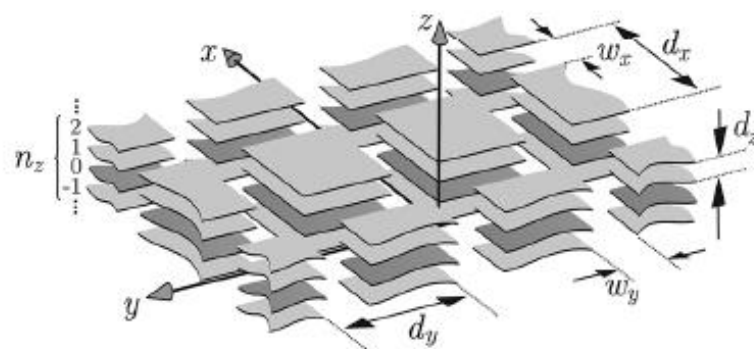
Figure 21: Multilayer configuration with the geometrical parameters

By applying the equivalence theorem, we derive an integral equation similar to the one obtained in (1).
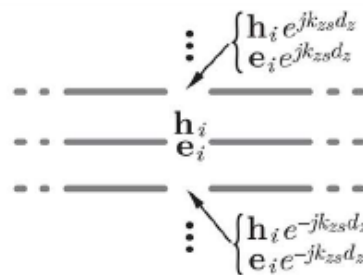
Step 1 : a plane wave propagating through the infinite layer stack generates magnetic and electric fields on the slots satisfying periodic boundary conditions along z.
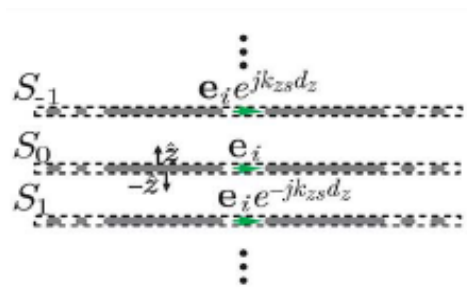
Step 2 : We apply the equivalence principle on the union of surfaces S_{nz} enclosing each layer.
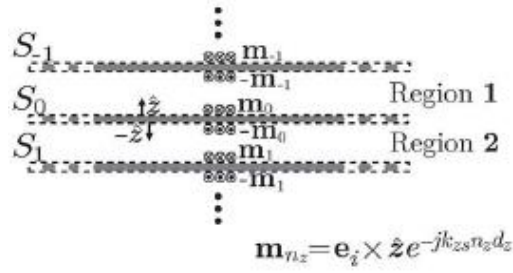
Step 3 : Equivalent magnetic currents are introduced on the apertures and PEC is filling the volume inside the surfaces.

$$\mathbf{m}_{n_z} = \mathbf{e}_i \times \hat{z} e^{-jk_{zs}n_z d_z}$$
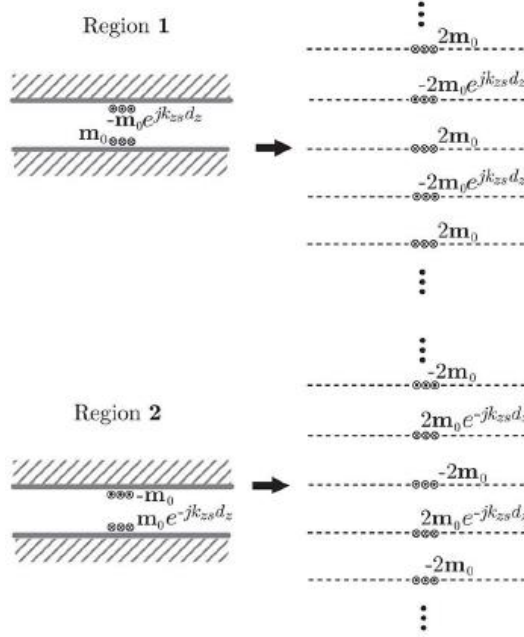
Step 4 : We apply the theorem image to replace the PEC with an infinite series of magnetic currents.

Then, we obtain the final integral equation by imposing the continuity of the total transverse magnetic field at the interface between both regions :

$$\sum_{n_z even} \int_{-\infty}^{\infty} \int_{-\infty}^{\infty} 4\mathbf{m}_0(\boldsymbol{\rho}')\mathbf{g}(\boldsymbol{\rho} - \boldsymbol{\rho}', n_z d_z, z = 0)d\boldsymbol{\rho}' \quad -$$

$$\sum_{n_z odd} \int_{-\infty}^{\infty} \int_{-\infty}^{\infty} 2(e^{-jk_{zs}d_z} + e^{jk_{zs}d_z})\mathbf{m}_0(\boldsymbol{\rho}') \times \mathbf{g}(\boldsymbol{\rho} - \boldsymbol{\rho}', n_z d_z, z = 0)d\boldsymbol{\rho}' =$$

$$2\mathbf{h}_i(\boldsymbol{\rho}, z = 0) \qquad (18)$$

since the interlayer distance is extremely small, we can do the following approximation of the exponential function in (18) : $e^{jx} \approx 1 + x$, after few algebraic steps, we obtain the new equation :

$$\sum_{n_z}(-1)^{n_z} \int_{-\infty}^{\infty} \int_{-\infty}^{\infty} 2\mathbf{m}_0(\boldsymbol{\rho}')\mathbf{g}(\boldsymbol{\rho} - \boldsymbol{\rho}', n_z d_z, 0)d\boldsymbol{\rho}' = \mathbf{h}_i(\boldsymbol{\rho}, 0) \qquad (19)$$

By applying the same procedure used in the single layer case, i.e. splitting the magnetic currents in TE,TM and coupling modes and using Galerkin projection we can

25

demonstrate that the mutual admittance between TE and TM currents can be neglected . The main difference with respect to the single layer derives from the higher Floquet modes of the Green's function to account for the infinite sum on the indexes. This infinite sum is written in closed form as : $\sum_{n_z=-\infty}^{\infty}(-1)^{n_z}e^{-jk_z|n_z|d_z} = j\,tan(\frac{k_z d_z}{2})$

The slot susceptance and the reactance of a layer in multilayer environment become :

$$B_{s\infty} = \frac{j2k_0}{\xi_0} \sum_{m_y \neq 0} \frac{\left|sinc(\frac{k_{ym}w_x}{2})\right|^2}{|k_{ym}|}\,tan\,(\frac{k_{zm}d_z}{2}) \qquad (20)$$

$$Y_{\infty,TM} = \frac{-j}{B_{s\infty}} \qquad\qquad Y_{\infty,TE} = \frac{-j}{B_{s\infty}\left(1-\frac{sin^2(\theta)}{2}\right)} \qquad (21)$$

A code has been implemented (Appendix B) in MATLAB in order to compare the capacitances of TE and TM incidence for both single isolated layer and multilayer configuration. The results obtained can be observed on the following curve:
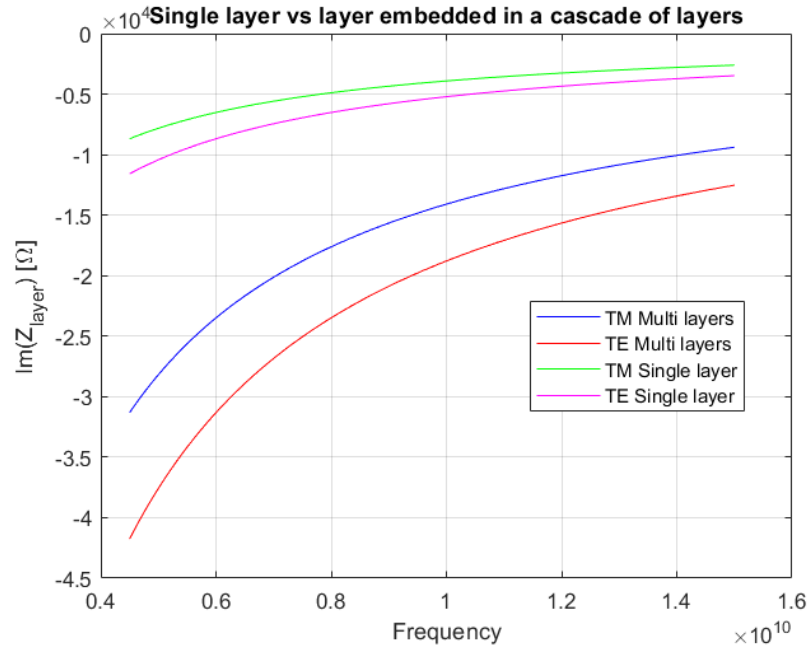

Figure 22: Equivalent capacitance of a layer embedded in a cascade of layers along z with period $d_z = 0.012\lambda_0$ for both TE and TM incidence from $\theta_i = 45°$ with parameters $w_y = w_x = 0.03\lambda_0$ and $d_y = d_x = 0.15\lambda_0$, λ_0 being the wavelength at the frequency $f_0 = 15GHz$.

26

As we can see, the equivalent reactance of the isolated layer has been also reported for comparison. And for the same geometrical parameters, the equivalent reactance of the isolated layer differs from the same layer in a multisheet configuration. This is due to the reacting coupling occurring between closely spaced layers.

It should also be mentioned that the convergence of the series (B_s and $B_{s\infty}$) is reached from **N=10.**

4.2.2.2. Infinite Periodic Array

From the previous study of the isolated and multilayer setup, the active input impedance of the connected arrays of slots can be predicted in advance thanks to the theoretical analysis. This analysis of course considers all the higher-order-mode interactions between adjacent layers composing the array plane and the ADL. The method here is based on an infinite periodic array. Then, the active input impedance of the array is expressed as follows :

$$z_{act} = -\frac{1}{d_x} \sum_{m_x=-\infty}^{\infty} \frac{sinc^2(k_{xm}\frac{\delta_s}{2})}{D(k_{xm})}$$

It consists in a infinite summation of Floquet modes with index m_x and wave numbers

$$k_{xm} = k_{x0} - \frac{2\pi m_x}{d_x} \quad and \quad k_{x0} = k_0 \sin(\theta)\cos(\varphi)$$

k_{xm} is the periodicity along x, k_0 is the propagation constant in free space, $\theta \; and \; \varphi$ are the angles towards which the array is pointing.

The periodicity accounting for the y-axis and for the stratification along z is the transverse connected array Green's function expressed as :

$$D(k_x) = \frac{1}{d_y}\sum_{m_y=-\infty}^{\infty} G_{xx}(k_x, k_{ym})J_0(k_{ym}\frac{w_s}{2})$$

With wave numbers $k_{ym} = k_{y0} - \frac{2\pi m_y}{d_y}$ and $k_{y0} = k_0 \sin(\theta)\sin(\varphi)$, k_{ym} being the periodicity along y-axis, J_0 : zeroth-order Bessel function, it is the Fourier transform of the transverse edge-singular magnetic current distribution along the slot, G_{xx} is the spectral Green's function and represents the x-component of the magnetic field

radiated by a x-oriented elementary magnetic dipole. It accounts for the stratification along z-axis and can be expressed in terms of current solutions of the equivalent transmission lines which represent the layers above and below the plane of the slots :

$$G_{xx}(k_x, k_y) = G_{xx,up}(k_x, k_y) + G_{xx,down}(k_x, k_y)$$

$$= -\frac{I_{up,TE}k_x^2 + I_{up,TM}k_y^2}{k_\rho^2} - \frac{I_{down,TE}k_x^2 + I_{down,TM}k_y^2}{k_\rho^2}$$

With $k_\rho^2 = k_x^2 + k_y^2$ and the currents at the plane z=0 are defined by :

$$I_{up,Ti} = \frac{1}{Z_{up,Ti}}; \qquad I_{down,Ti} = \frac{1}{Z_{down,Ti}} \ and \ Ti \ \in \ \{TE; TM\}$$
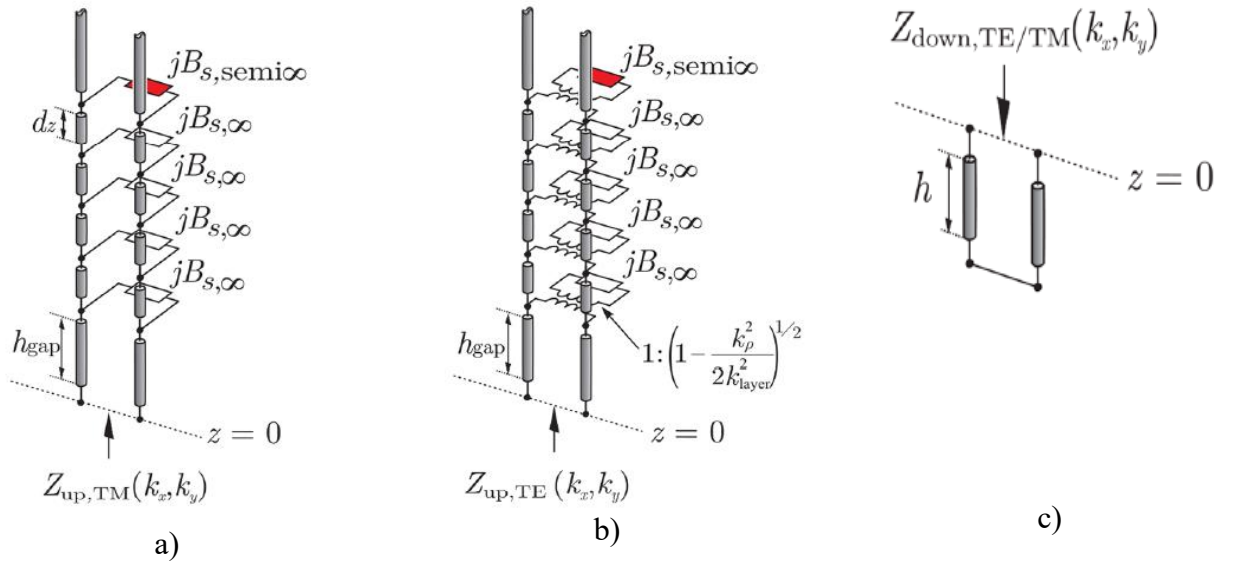
Figure 23: Equivalent transmission line model of a 5 layers SLAB for a generic a) TM b)TE plane wave c) equivalent shorted line representing the backing reflector

$Z_{0TE} = \xi k/k_z$ and $Z_{0TM} = \xi k_z/k$ are the characteristic impedances of the transmission lines for TE and TM incidence, $\xi \ and \ k$ are respectively the impedance and the wavenumber of the dielectric slab host with $k_z = \sqrt{k^2 - k_{x0}^2 - k_{y0}^2}$.

The term k_{layer} of the transformer is the propagation constant of the host medium in which the layer is embedded .

It has already been demonstrated in the previous section (equation 20) that each layer has an equivalence susceptance of $B_{s\infty}$. For the top layer, a semi-infinite solution is considered in

order to take into account the finite height of the ADL. The expression of the semi-infinite solution is given by :

$$B_{s,semi-\infty} = \frac{k_0}{\xi_0} \sum_{m_y \neq 0} \frac{\left| sinc(\frac{k_{ym}w_x}{2}) \right|^2}{|k_{ym}|} \times \left(1 + jtan\left(\frac{k_{zm}d_z}{2} \right) \right)$$

All the equations of this subsection have been implanted in MATLAB (appendix) and the 5 layers ADL has been designed and simulated in CST, the structure is depicted in figure 14 and the geometrical parameters are reported in table below.

$d_x = d_y$	w_s	δ_s	h_{gap}	d_{ADL}	w_{ADL}	d_z	h
$\dfrac{\lambda_0}{2.15}$	$\dfrac{\lambda_0}{47.5}$	$\dfrac{\lambda_0}{11.1}$	$\dfrac{\lambda_0}{78.7}$	$\dfrac{\lambda_0}{10.7}$	$\dfrac{\lambda_0}{111}$	$\dfrac{\lambda_0}{157.3}$	$\dfrac{\lambda_0}{12.5}$

Table 1: Dimensions of the unit cell in fig.14

The results are reported in the following curves :
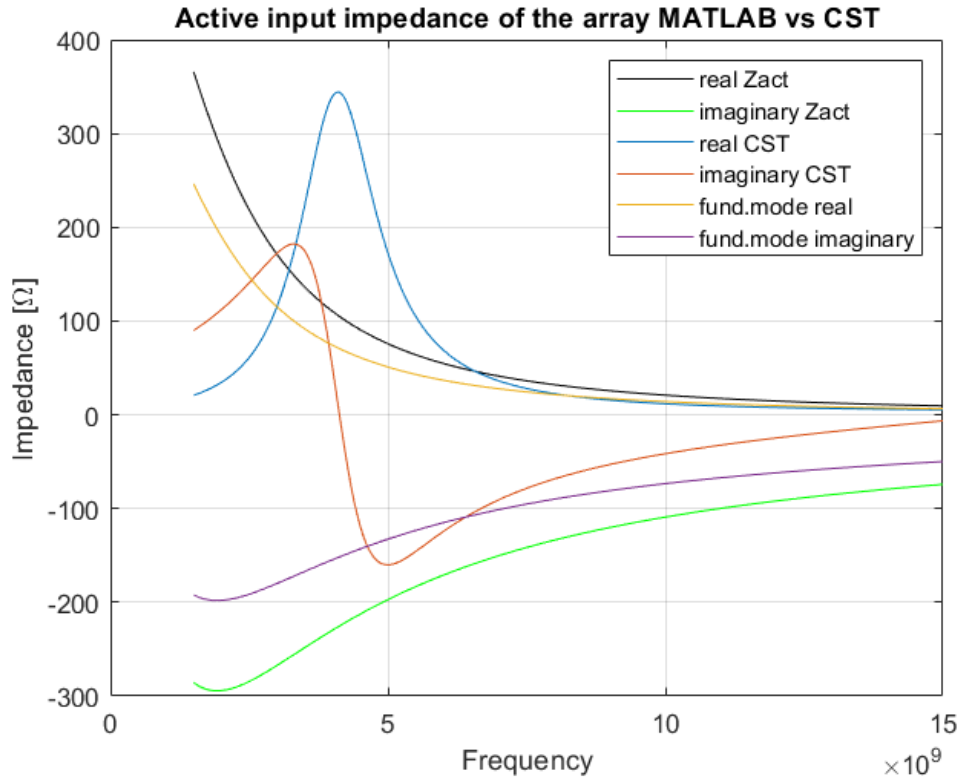
Figure 24: Input impedance of the connected array of slots loaded with a 5-layers ADL

CST vs MATLAB

Some differences can be observed between the two results, in practice they are supposed to match. Theses differences observed derive from the fact that the impedance of the slot is not taken into account in the MATLAB code, in the plane z=0 we should have the impedance of the slot. Therefore, the equivalent impedance of the upper stratification is added with the impedance of the slot.

5. Connected Slot Array with ADLs: A 6-15 GHz prototype

5.1. State-of-The-Art

5.1.1.   Composition

The unit cell of our antenna is composed of a slot in the presence of a backing reflector and loaded with ADLs. Three ADL slabs are used to perform a broadband transformation between the free-space impedance and the slot active input impedance. The ideal configuration presented in figure 25 below where the first slab has a permittivity of $\varepsilon_r = 2.2$ and the two others substrate have permittivity $\varepsilon_r = 1$:

Figure 25: Unit cell of connected array of slot loaded with ADLs. a) full stack of the three Slabs
b) view of spacers c) slot+ reflector view d) geometrical parameters

The slabs structure could be very bulky and heavy at low frequencies. For this reason, we resort to this structure where there is a backing reflector which ensure that the waves radiated in lower half space of the slot are redirected in the upper half space. Moreover, the configuration depicted is an ideal one. Therefore, the practical realization of the multi-layer PCB will require the use of standard substrates and additional bonding layers.

5.1.2.   Types of excitation

In microstrip antennas, types of excitation are classified in two categories. The one is contacting and the other one is non-contacting. In contacting methods, the power is routed to radiating patches using contact element such as coaxial cable and microstrip line. In the second feeding class, electromagnetic coupling is used to transmit the power of the microstrip line to the radiating patches. The four most types of feeding techniques used are: coaxial probe, microstrip line, aperture coupled, and proximity coupled.

- **Coaxial Probe Feed :** in this technique, the inner conductor of the coaxial cable is connected to the microstrip patch of the antenna and the outer one is connected to the ground plane. The advantages of coaxial probe are the minimization of radiation, easy fabrication, and efficient feeding.
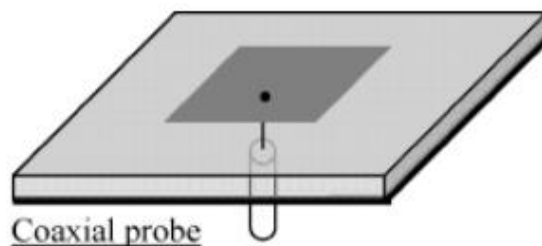

Figure 26: Coaxial probe feed

- **Microstrip Line Feed :** in this feeding method, the microstrip patch(or slot) is directly connected to the conducting microstrip feed line. The dimensions of the line differ from those of the patch. Easy fabrication and matching.
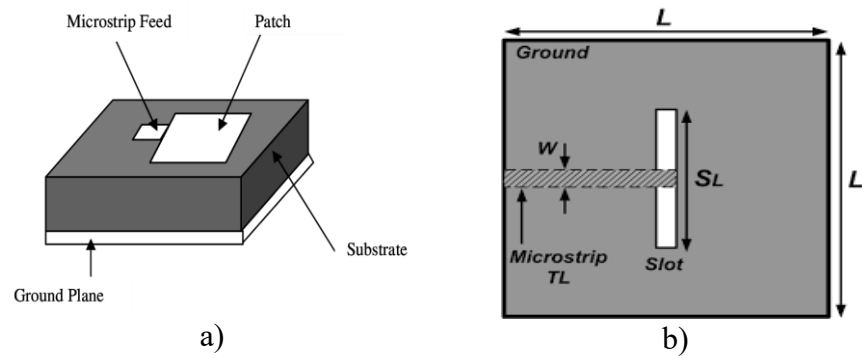

Figure 27: Microstrip Line feed a) patch b) slot

- **Aperture Coupled Feed :** it is consisting in two different substrates separated by a ground plane. the microstrip patch and the feed line are coupled through a slot in the ground plane. The advantages of this excitation are minimization of interference and pure polarization.
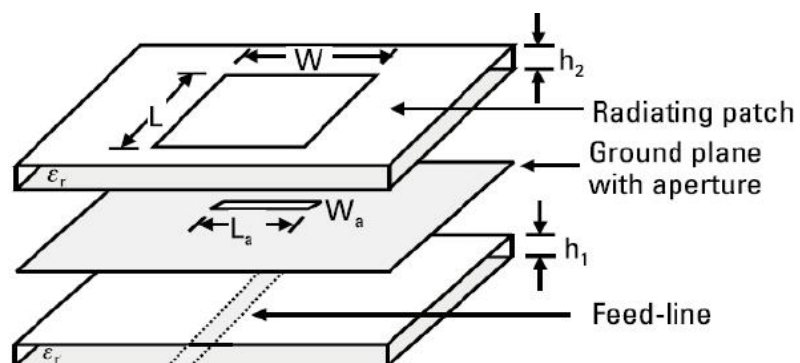

Figure 28 : Aperture couple feed

32

- **Proximity Coupled Feed :** Comparatively to the previous methods, the fabrication of that one is a bit complicated. It uses two dielectric substrates where the patch is at the upper surface of the top substrate and the feed line is between the two substrates. It provides large bandwidth and avoids spurious radiation.
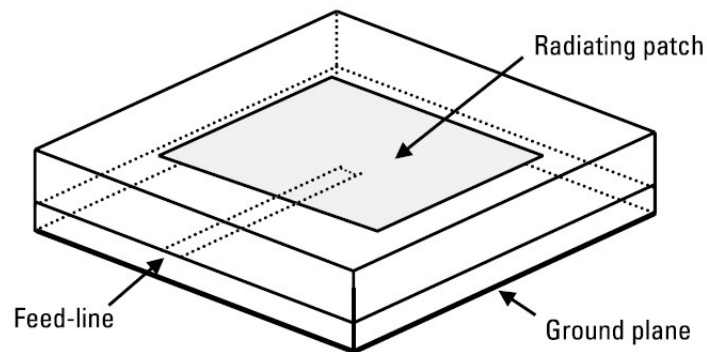

Figure 29 : Proximity Coupled Feed

5.2. Practical Study

5.2.1.   Simulation Platform: CST MWS Studio Suite

Why a numerical tool ?

A numerical tool is required for the simulation of antennas and in general for 3D designs because simulation is the crucial process before any realization since we need to study the performances of the systems to find out the different problems we may encounter and also examine the results. The simulation allows us to avoid errors during manufacturing and test the structures on a computer before initiating the physical implementation which allows us to reduce the production costs.

CST MICROWAVE STUDIO?

CST MICROWAVE STUDIO is a specialist tool for 3D EM simulation of high frequency components. It enables the fast and accurate analysis of high frequency(HF) devices such as antennas, filters, couplers, planar and multi-layer structures. CST MWS is based on the finite integration technique (FIT), a very general approach which describes Maxwell's equations on

33

a grid space and can be written in time domain as well as in frequency domain and is not restricted to a certain grid type. Many results available at once, parametric approach and speed are the main advantage of CST MWS. However, a complexity of work and creation of structures having large design details so that the simulation could take several hours up to several days sometimes, especially if the project to be simulated is of a relatively large volume and has many details.

USER INTERFACE
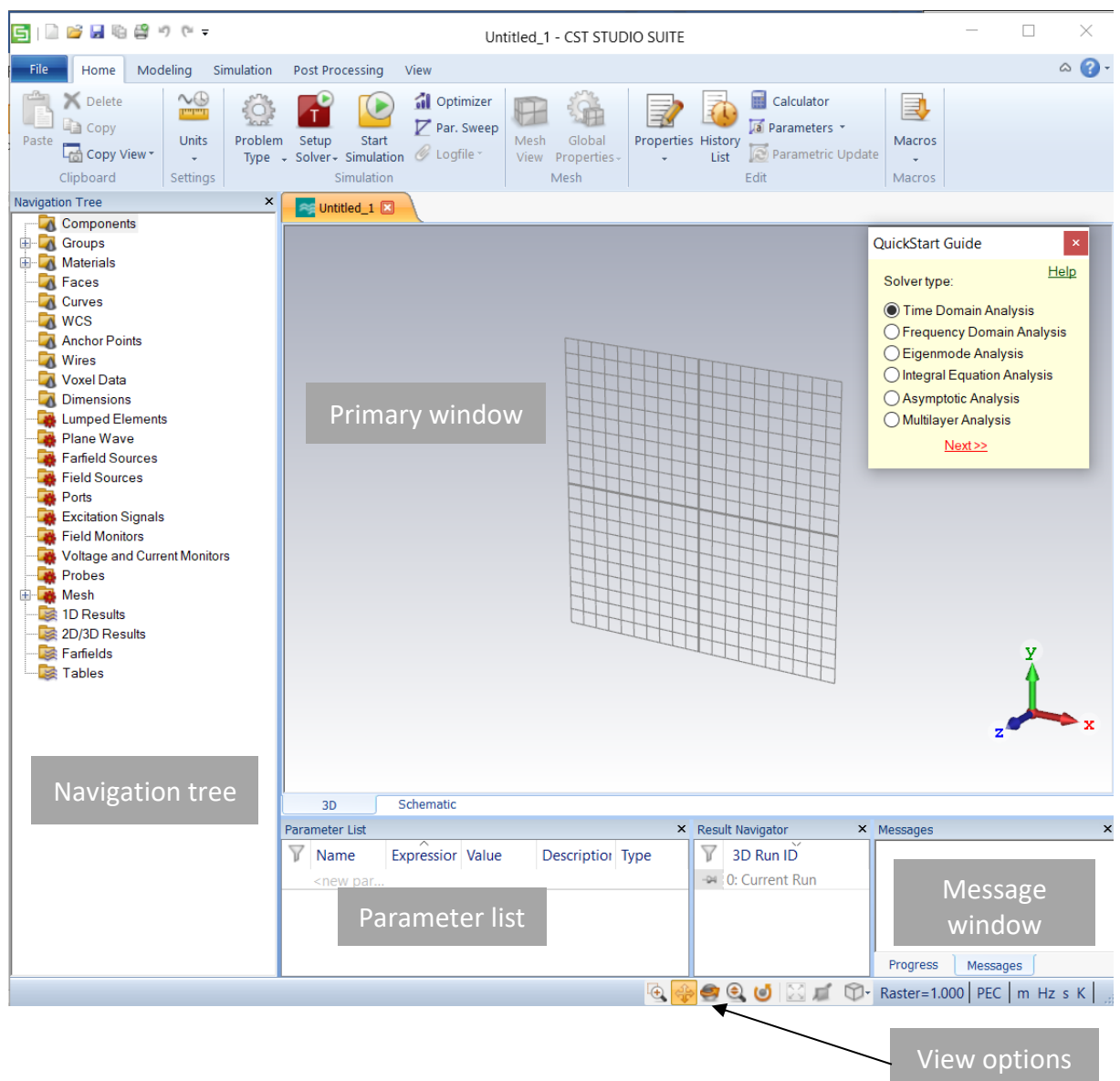
QuickStart guide : it is a step by step guide that helps to build antenna easily (strongly recommended for new users).

HOW TO BUILD ANTENNA (1)
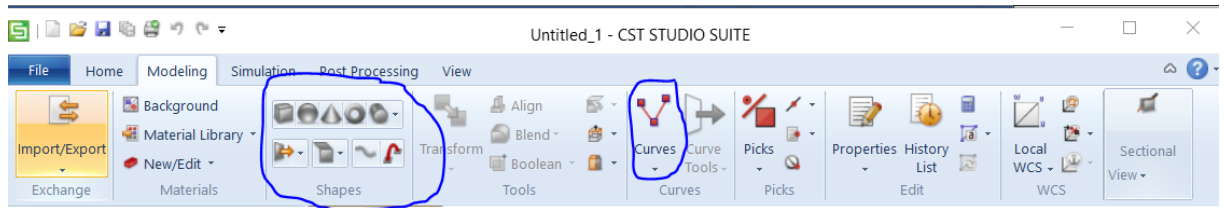
Modelling menu → Select shape (brick, cylinder, torus…) → press ESC to open dialog window → insert all data → preview and confirm.

Geometrical transformations(rotate, scale…), Boolean operations(add, subtract…) and additional actions (extrude, blend, etc) can be used to generate more complex structures from basic solid shapes.

As an alternative, a curve can also be defined as a starting point if we want to design a specific profile.

HOW TO BUILD ANTENNA (2)
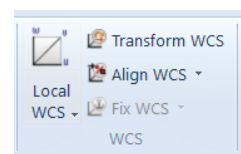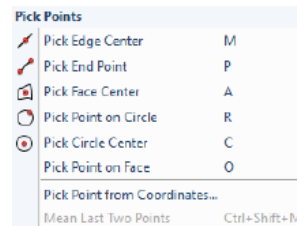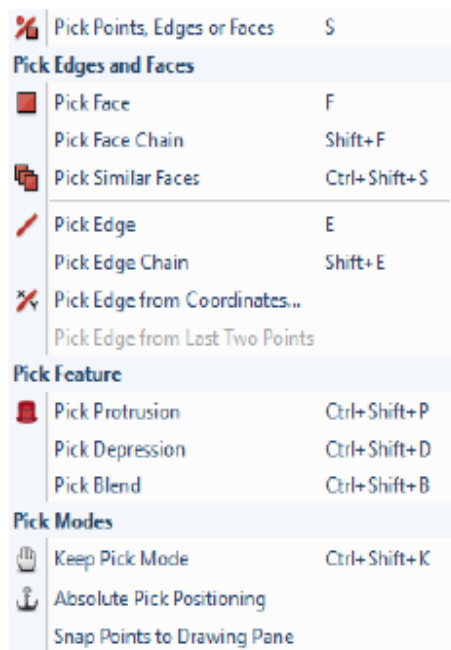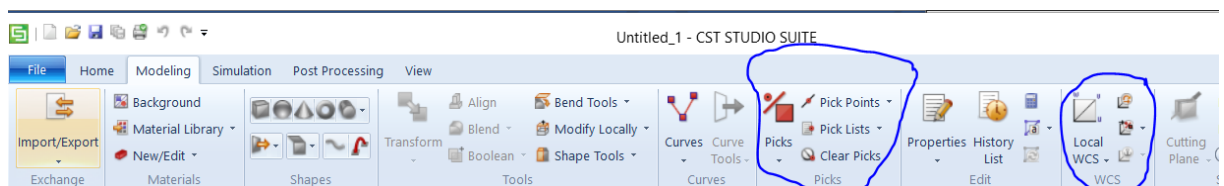
Simple elements(points, edges, faces…) can be picked to enforce some of the aforementioned operations.

A local coordinate system can also be used to facilitate the construction of the structure (stack operation for instance).

PORT DEFINITION
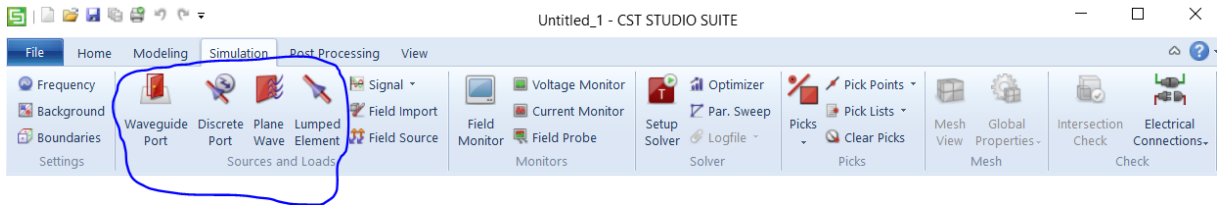
Discrete ports can be used for TEM-like modes not for higher modes. It is strongly recommended to use waveguide ports whenever it is possible because they provide better match to the mode pattern and higher S-parameters accuracy.
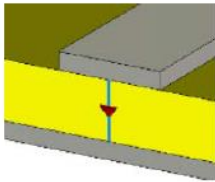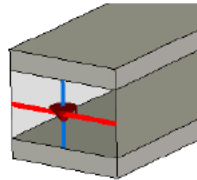
Discrete edge port   Discrete face port   Waveguide port
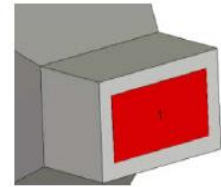
Discrete face ports are more precise than discrete edge ports.

BOUNDARIES AND SYMMETRIES

MWS defines a bounding box surrounding the simulation domain on whose 6 contour surfaces boundary conditions have to bet set.

Electric : no tangential electric field at surface (Et=0)

Magnetic : no tangential magnetic field at surface (Ht=0)

Periodic

Unit cell

	Free space (open)		Electric conductive wall with finite conductivity (conducting wall)
	Free space with some extra farfield calculations (open add space)		Most of the time, boundaries are set as **open add space** for Antennas.

Symmetries (electric/magnetic) can be applied to speed up the simulation time.

MESH
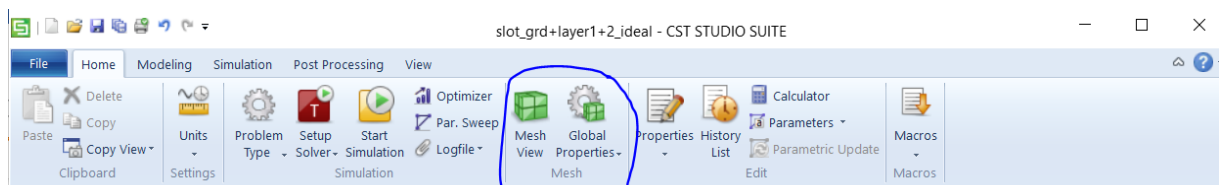
A mesh is chosen automatically by the software and can be refined by choosing the adaptative mesh refinement in global properties box.

SOLVERS
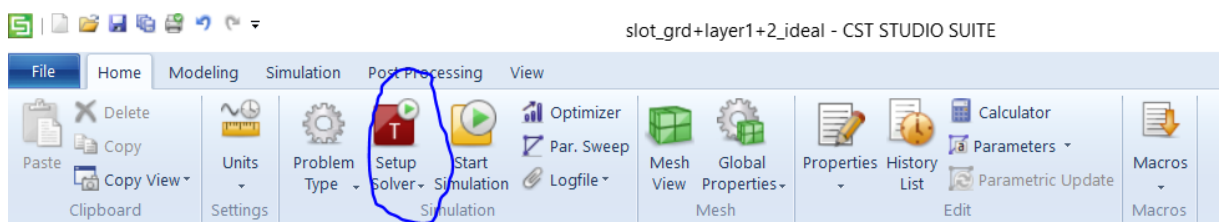
In general, the time and frequency domain solver could be used for most of all the applications. The frequency domain solver is better used for narrow band and single frequency problems. The eigenmode solver is a specialized tool for strongly resonant structures and narrow band cavities. The integral equation solver is intended for large structures. The asymptotic solver is used for RCS (radar cross section) measurement and antenna farfield calculations. The multilayer solver is suitable for layered geometries.

37
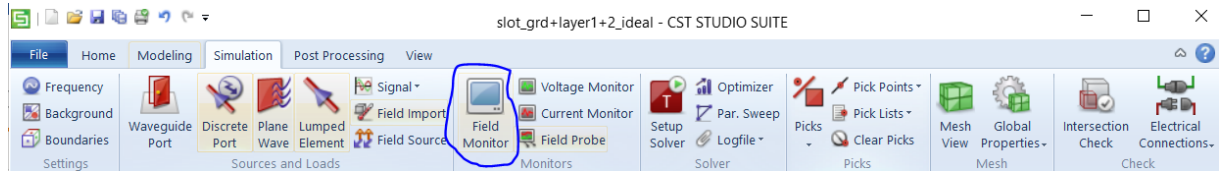
MONITORS

Monitors must be defined before simulation and provide a set of 2D/3D results.
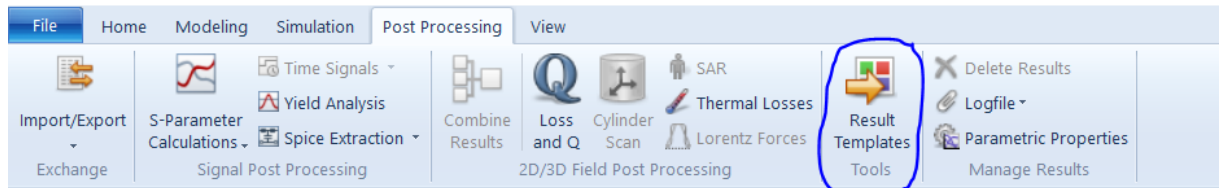
Template based post processing allow to get specific results derived directly from the main antenna or from the monitors defined. They are very useful to store all the results, especially in case of parametric seeps.

RUN A SIMULATION / PARAMETRIC SWEEP
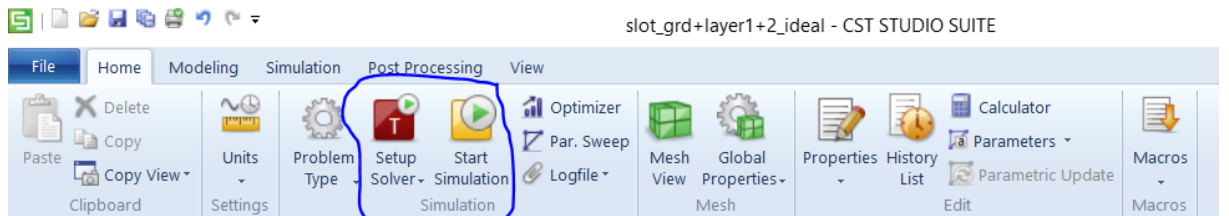
The accuracy of the simulation can be set by opening the solver's properties and choosing the level of accuracy desired. Typically, the T-solver is set at -40dB . Moreover, if the design is realized with parametric numbers, one may speed up the optimization by running a parametric sweep of one or few variables.

HISTORY LIST
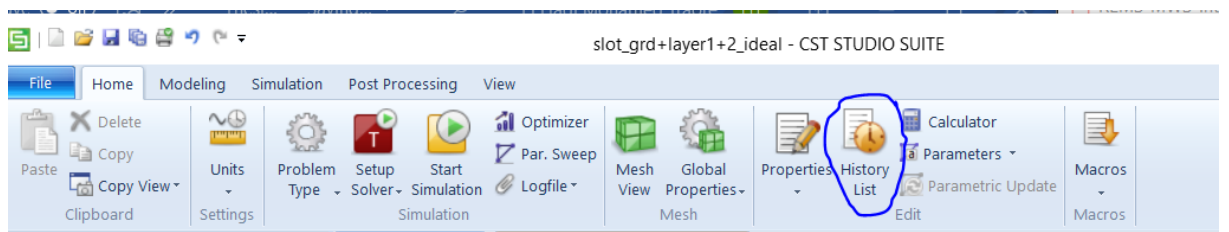
All actions performed during a MWS project are stored in a history list and can be accessed to do modifications like edit, delete, hide or unhide some instructions.

5.2.2.   Antenna Element Design

In the practical design of the antenna, bonding layers are included to enable the realization of the multi-layer PCB. Therefore, several Rogers substrates are used to bond the different layers of the first slab ($\varepsilon_{r1} = 2.2$, thickness $t_1 = 0.127mm$). It ensures very small inter-layer spacing which would be too demanding for foam substrates. The Slabs are bonded together with Arlon CuClad 6700 ($\varepsilon_{r6700} = 2.35$, $t_{6700} = 0.038mm$) and Rohacell foam($\varepsilon_{r2} = \varepsilon_{r3} = 1.06$) is used for the two other slabs . Since foam cannot be metalized, the patches will be printed on a thin dielectric film of LG4014($\varepsilon_{r4014} = 2.9$, $t_{4014} = 0.050mm$) and this latter will be glued to the foam using adhesive Arlon CuClad 6250($\varepsilon_{r6250} = 2.35$, $t_{6250} = 0.038mm$).

Figure 30: stackup of the unit cell array with bonding layers a) 2D view b)3D view

Regarding the complexity of the structure, it requires a smart approach to realize the design with smoothness and no mistakes. Therefore, the general idea of the design is to follow the stackup depicted in figure 28 a). For the ADLs, apply transformations along z to replicate the layers. The dimensions of the design are filled in the tables below :

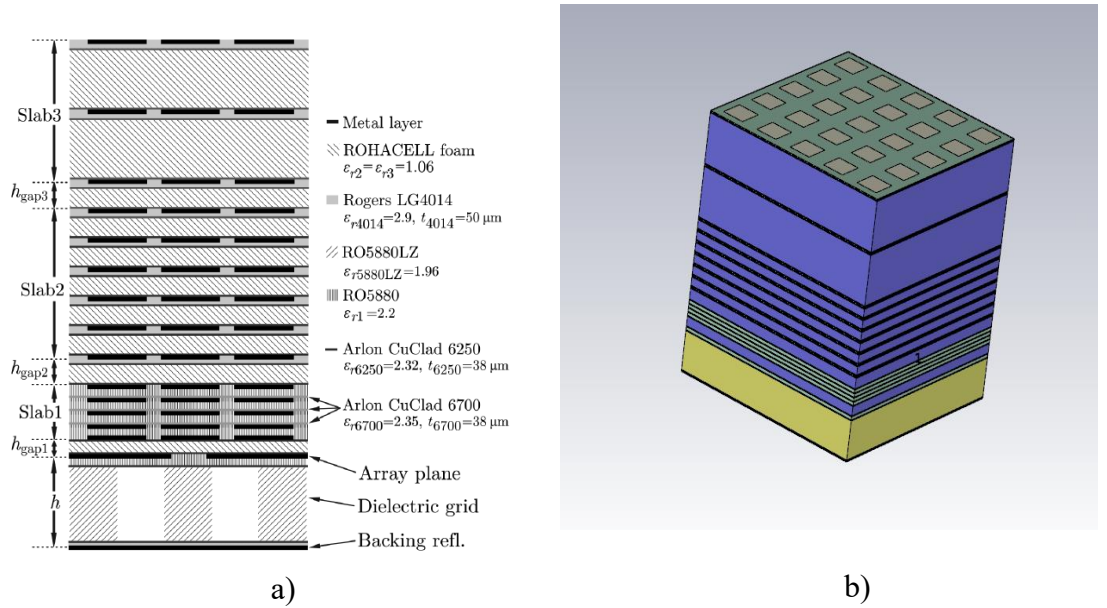| Parameters	Description	Unit	Slab1	Slab2	Slab3
d_{ADL}	W&L of patch	mm	1.862	1.862	1.862
w_{ADL}	Gap between two patches	mm	0.19	0.2	0.4
h_{gap}	Inter-slab distance	mm	0.424	0.474	2.1
d_z	Inter-layer distance	mm	0.127	0.33	2
n_z	Number of layers		5	6	3
ε_r	Dielectric constant		2.2	1	1

Table 2: Dimension of ADLs

Parameters	Description	Values [mm]
$d_x = d_y$	Period of the unit cell	9.31
w_s	Width of the slot	3.8
h	Distance reflector to slot	2.0

Table 3: Dimensions of the single-polarization connected array

5.3. Tasks Performed

5.3.1. Design of the Dielectric Grid

To enable the possibility of implementing the feeding structure with PCB through-hole technology, we first consider a dielectric substrate (RO5880LZ) of permittivity $\varepsilon_r = 1.96$ between the backing reflector and the slot plane. But it has been shown that when compared to a foam substrate, such a slab degrades the matching performance of the array. Therefore, we have to reduce its effective permittivity. To do so, the dielectric can be perforated to realize grid configuration. The permittivity of this structure is expected to be $\varepsilon_r = 1.5$. A substrate of permittivity $\varepsilon_r = 1.4$ can also be used since there is no big differences between both.

In the ideal approach, we could just design a dielectric slab and create a material of permittivity equal to 1.4 or 1.5. However, in the realistic design, we will use existing dielectric substrates.

In practice, we construct the ideal substrate of permittivity 1.4 or 1.5 and also the perforated dielectric of RO5880LZ ($\varepsilon_r = 1.96$). After that we simulate both of them by using the eigenmode solver to get the Cut off frequencies and we compare these frequencies. If they are similar, then the perforation is good, otherwise the perforation is adjusted, and we repeat the same procedure.

This task has been realized in CST and the results obtained can be see on the following curves:
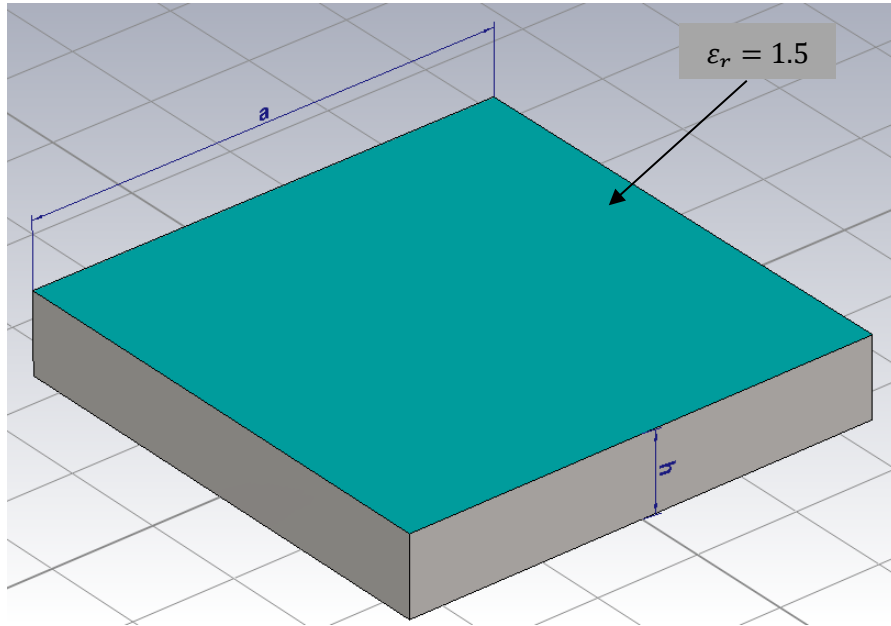

Figure 31: Dielectric Slab of permittivity $\varepsilon_r = 1.5$
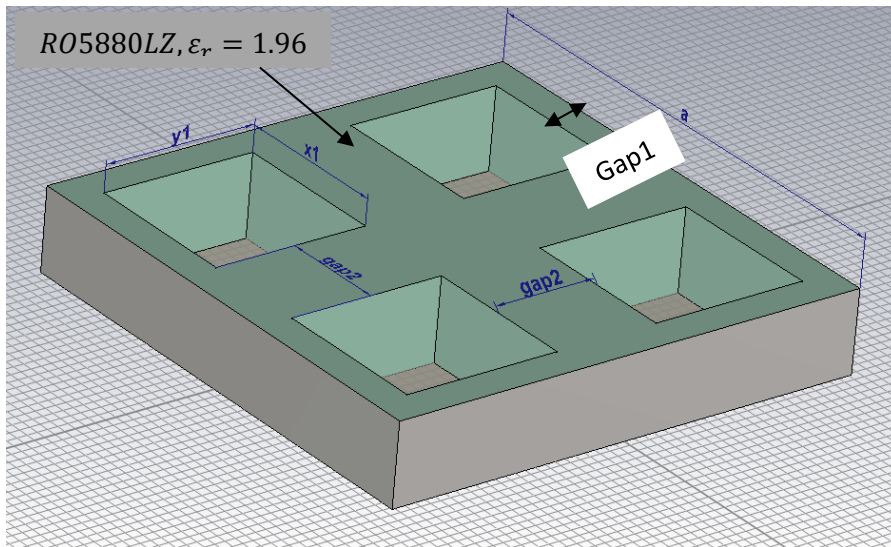
Figure 32: Equivalent grid configuration

Parameters	Values (mm)
a	9.31
h	1.559
X1	3
Y1	3
Gap 1	0.655
Gap 2	2

Table 4:Sizing of the grid structure

Cut off frequency (GHz) / Mode	$\varepsilon_r = 1.4$	$\varepsilon_r = 1.5$	Grid config
1	19.24	18.59	17.73
2	30.42	29.40	29.46
3	30.42	29.40	29.46
4	38.48	37.18	38.62

Table 5: Cut off frequencies of the dielectric substrate of RO5880LZ milled in grid configuration vs dielectric slab of material with permittivity $\varepsilon_r = 1.4$ and $\varepsilon_r = 1.5$

The structure being symmetric, the results can be limited to the first four modes. Therefore, we obtained the aforementioned results in table 4. These results show good agreement between the grid substrate designed and the uniform substrate of permitivity $\varepsilon_r = 1.5$. Furthermore, the substrate of permittivity $\varepsilon_r = 1.4$ could also be used according to the simulations since the differences are negligible.

5.3.2.   Design of the feeding Structure

Microstrip feed line is implemented to feed each slot of the connected array. The microstrip line is terminated by a shorting via and a microstrip to co-coaxial transition is designed in order to feed the elements with integrated coaxial cables. To ensure that the feeding line is working perfectly, the overall network is designed in isolation and the transmission coefficient between the two ports is observed.
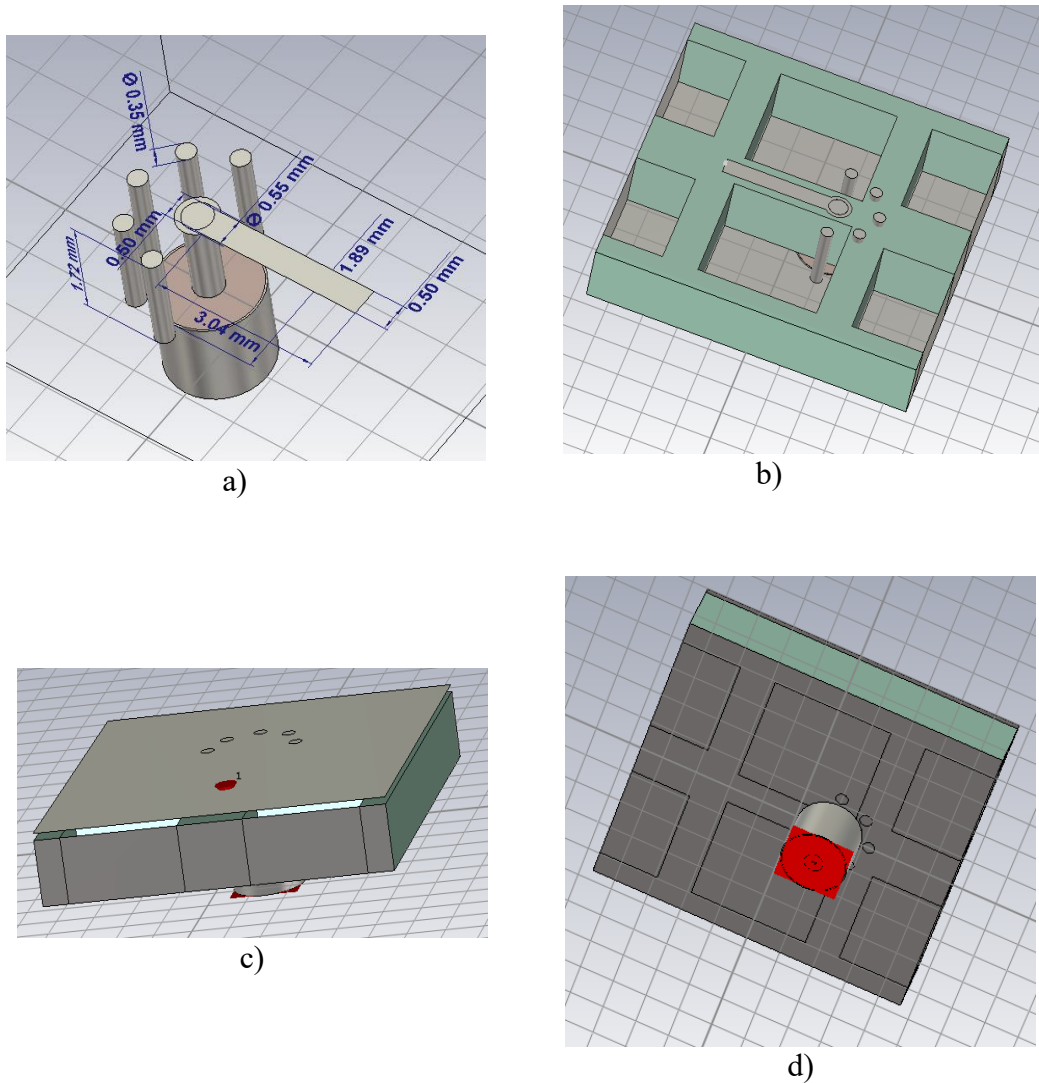
Figure 33: Microstrip to-coaxial transition a) geometrical parameters b) top view

c) port 1 d) port 2

Transmission coefficient S_{12} : considering a two-port network, S_{12} represents the power received at port 2 relative to the power input to port 1, for example $S_{12} = 0$ implies that all the power delivered at port 1 ends up at the terminals of port 2.

The feeding network designed in figure 33 is then supposed to transmit the maximum of power available at port 1 to port 2 (or vice versa).

Let us examine the transmission coefficient obtained after the simulation of the network in isolation :
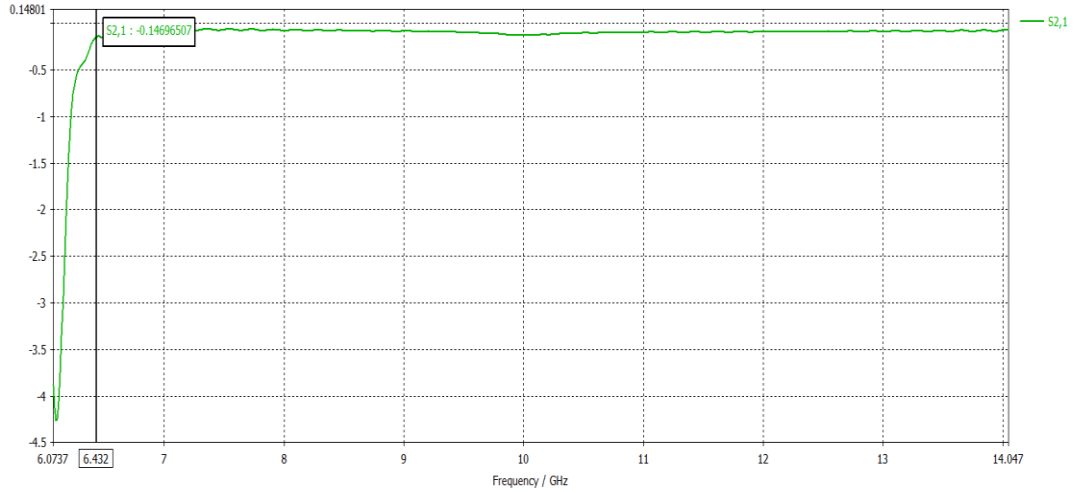
Figure 34: Transmission coefficient between port 1 and port 2

The transmission coefficient is higher than -0.15 dB from 6.4 GHz to 15 GHz, which means that about 97% of the power delivered at port 1 is transmitted to port 2 over the 6.4-15GHz bandwidth. Therefore, one can assume that the feeding structure is well designed.

5.3.3. Infinite Array Simulation

In this section, the model is based on the infinite array by assuming the slots to be infinitely periodic along both y and x-directions. Moreover, this is an ideal case to observe the behaviour of the centered unit cell.

Before analysing the results obtained in the simulations, it is preferable to define some antenna parameters to be more familiar with them in the following.

Return loss (S11) : it is the loss of power in the signal reflected by a discontinuity or a mismatch in a transmission line. In a single polarization (one port) it is called S11.

VSWR : it stands for Voltage Standing Wave Ratio. It is a function of the return loss which describes the power reflected from the antenna. If the return loss (also called reflection coefficient) is given by S11, then the VSWR is defined by the following expression :

$$VSWR = \frac{1 + |s_{11}|}{1 - |s_{11}|}$$

It is always a real and positive number for antennas, the smaller it is the better the antenna is matched to the transmission line and more power is delivered to the antenna.

44

Bandwidth : it is the range of frequencies over which the antenna can operate properly . Let us consider F_M, F_m, F_c respectively the highest, lower and center frequency of the band, then the bandwidth is defined as :

$$BW = 100 \times \frac{F_M - F_m}{F_c}$$

Directivity : it is a fundamental antenna parameter that measures the ability of an antenna to concentrate energy in a certain direction. High directivity implies a directional antenna and an antenna that radiates equally in all direction would have zero directionality.

Gain : it is the ratio of the radiation intensity in a given direction to the radiation intensity that would be obtained if the power were radiated isotropically (same radiation in all directions). It describes how much power is transmitted in the direction of peak radiation. Comparatively to the directivity, it considers the actual losses occurring. It is a function of the directivity and expressed as the following :

$$G = kD$$

Where $0 \leq k \leq 1$ account for dissipative losses.

Radiation Efficiency : it is the ratio of power radiated (P_{rad}) by the antenna to the power delivered (P_{input}). A high efficiency antenna has most of the power present at the antenna's input radiated away while a low efficiency antenna has most of the power absorbed as losses within the antenna or reflected away due to impedance mismatch. It is expressed as :

$$\varepsilon_R = \frac{P_{rad}}{P_{input}}$$

The efficiency is commonly quoted in terms of percentage or in decibels (dB).

Results Analysis

A first type of centered slot is chosen and fed with a microstrip line terminated by a capacitor modelled by a square patch and connected to the coaxial connector. The connector is placed at $x_{pos} = 2mm$ from the origin and perpendicular to the slot, the line dimensions are $L = l + x_{pos}$ with $l = 2.3mm$ and $W = 0.4mm$, the square patch connected at the end of the line is a $l_c \times l_c$ square with $l_c = 2mm$.

The feed is placed under the slot at a distance $t = 0.254mm$ from the slot.
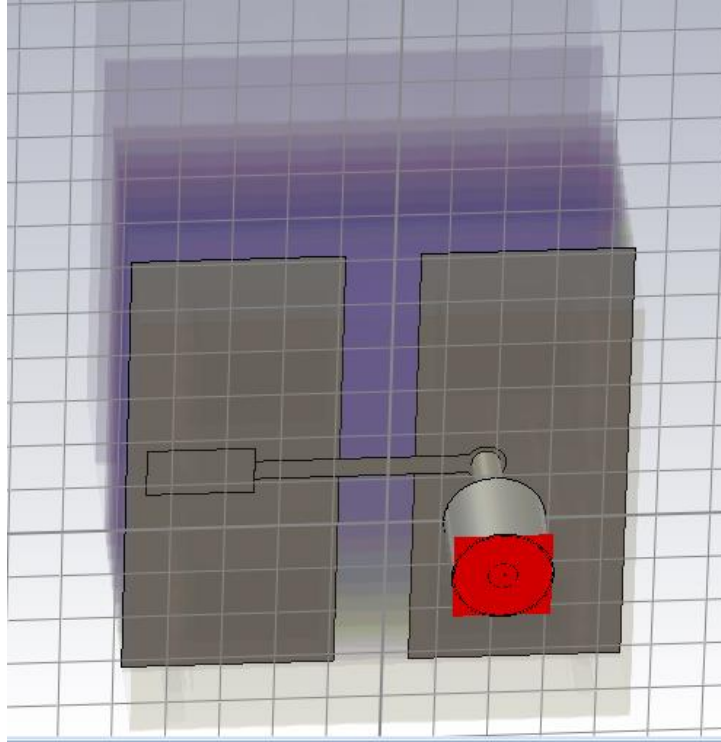
Figure 35: First shape of the slot

Before running the simulation, we must ensure that the boundaries satisfy the infinite array condition. This operation is done by setting the right boundaries: Apply PEC(Perfect Electrical Conductor)and PMC (Perfect Magnetic Conductor) conditions or use periodic boundaries conditions to replicate the unit cell along x and y axis. PMC is applied along the slot direction and PEC in the orthogonal direction.
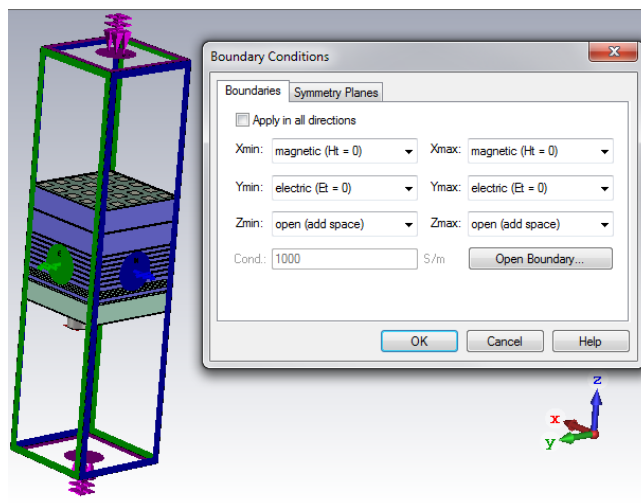
Figure 36: PEC/PMC conditions

S-Parameters [Magnitude in dB]
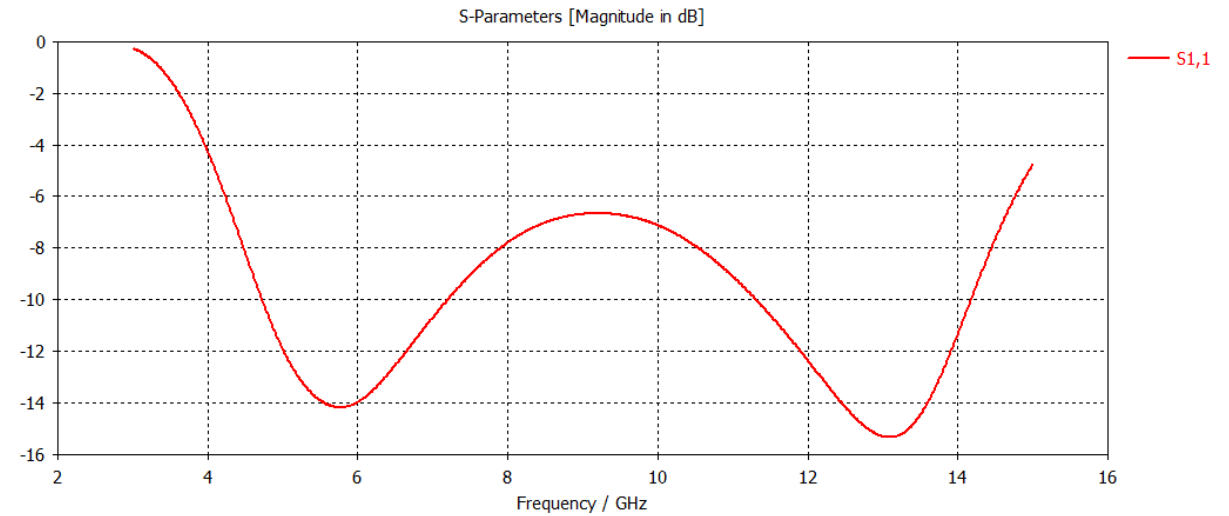
Figure 37: Return loss

Even if the dual band effect is visible ($S_{11} < -10dB$ in 6GHz and 14GHz band), the structure has to be optimized to improve the wideband performances. To do so, the slot is tapered into a special shape and the square patch of the feed is optimized into a rectangular $l_c \times l_x$ patch where $l_c = 1.5mm$ and $l_x = 1mm$. The new structure of the slot is shown in the figure below :
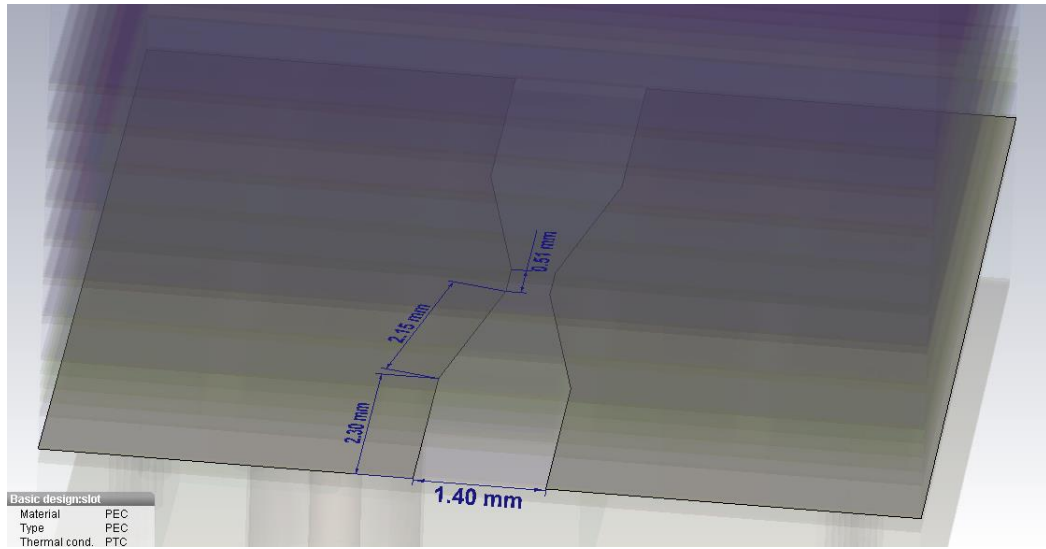
Figure 38: Tapered slot with its dimensions

The new reflection coefficient obtained is :
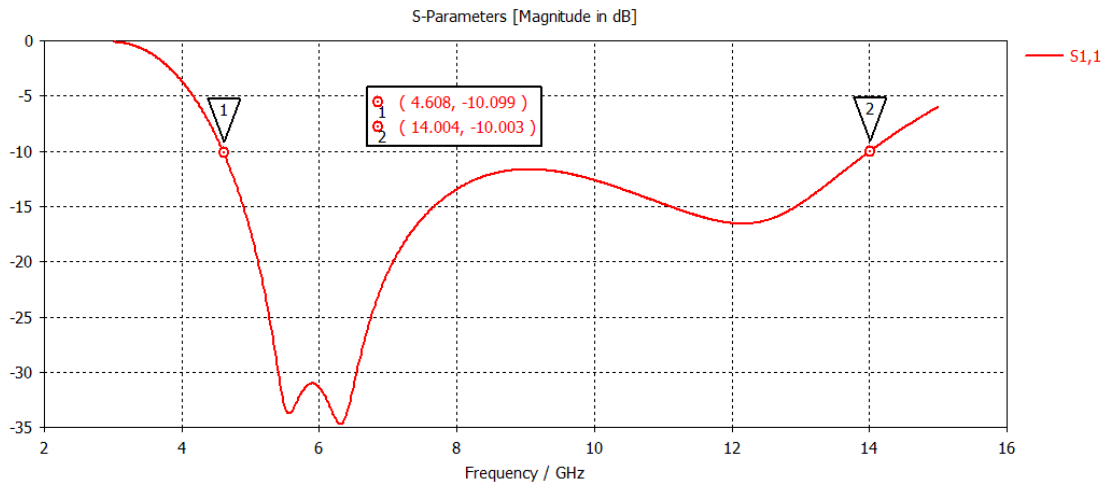
Figure 39: Return loss of the prototype in infinite array configuration

From the curve, it can be observed that the return loss is less than -10 dB from **4.608 GHz** to **14 GHz**, thus we get an overall bandwidth of **9.392 GHz.**

Besides, the VSWR is also plotted :
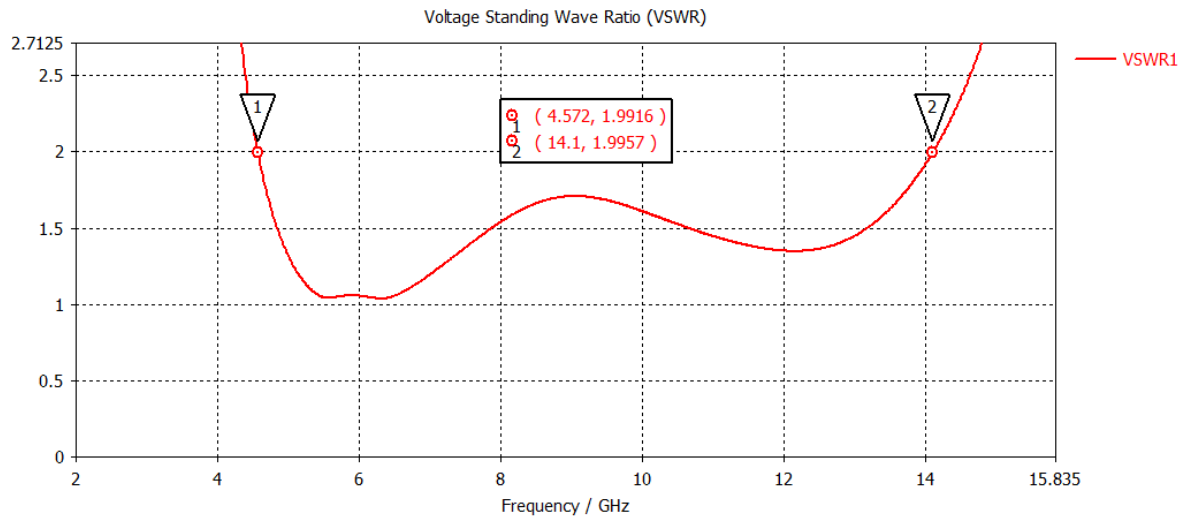
Figure 40: VSWR of the prototype in infinite array configuration

VSWR < 2 between 4.572 GHz and 14.1 GHz, **BW= 9.528 GHz.** The minor difference between the previous one calculated is due to the fact that VSWR < 2 corresponds to $S_{11} < -9.5\ dB$.

In conclusion, the wideband performance is achieved in the infinite array configuration. Additional informations on the performances are shown in the following :

48
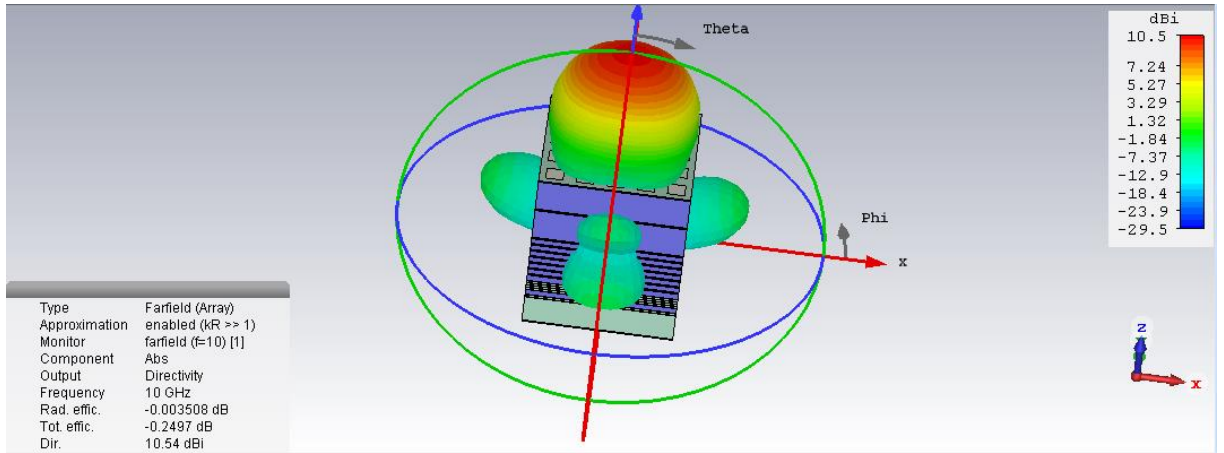
Figure 41: 3D radiation pattern at 10 GHz
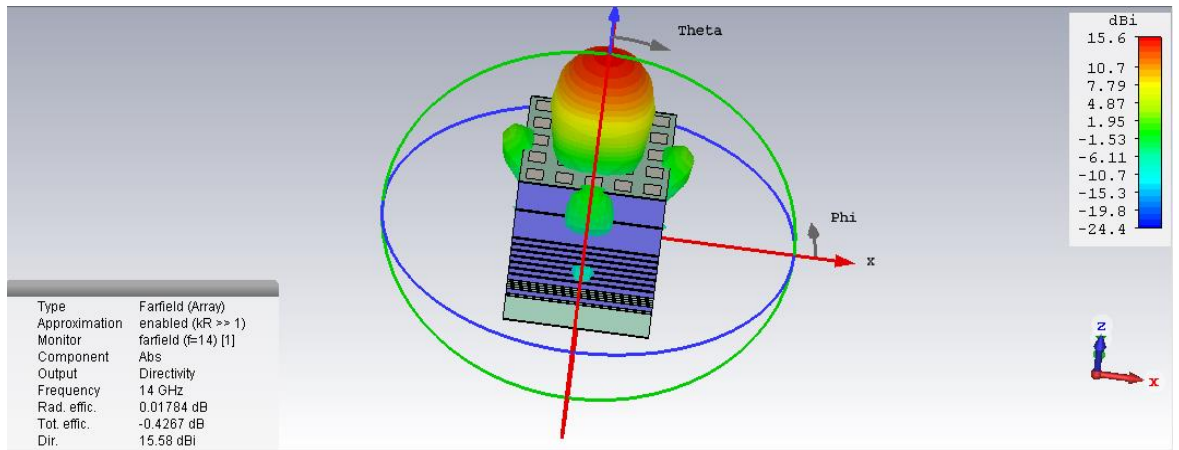
Figure 42: 3D radiation pattern at 14 GHz

For sake of brevity, all the antenna's parameters are consigned in a single table :

	Directivity [dBi]	Realized Gain [dB]	Total efficiency[dB]	Total efficiency [%]
10 GHz	10.54	10.29	-0.2497	94
14 GHz	15.58	15.15	-0.4267	90

Table 6: Farfield Performances of the prototype for normal incidence

The global efficiency of the antenna is quite good since the total efficiency takes into account the impedance mismatch at the port and the variation between directivity and gain is very low. The presence of side lobes in the radiation pattern does not affect the performances of the antenna because the main lobe is radiating at 0 degree and the side ones are not directed in that direction and their magnitude is also negligible.

49

6. The 26-39GHz dual band antenna

As said at the beginning of the project, the first antenna was designed as a prototype and the purpose was to play on the size of that one to improve the frequency bands performances. From the previous chapter, it was shown that the prototype achieves good performances in terms of bandwidth, gain, directivity, and efficiency. Therefore, we can divide all the dimensions of the structure so that it works in the desired frequency band. Then, dividing by three, in theory we should get approximately a bandwidth of 27 GHz spread over 13-42 GHz. The new dimensions of the design are :

Parameter List

Name	Expression	Value	Description	Type
t1	= 0.127/3	4.23333333333333e-02	thickness roacell RO880	Length
t6700	= 0.038/3	1.26666666666667e-02	thickness arlon cuclad 6700	Length
t6250	= 0.038/3	1.26666666666667e-02	thickness arlon cuclad 6250	Length
t4014	= 0.050/3	1.66666666666667e-02	thickness rogers LG4014	Length
hpr	= h-(t1+t6700+2*t6250)	0.586333333333334	thickness dielec back	Length
hgpr	= hgap1-2*t6250	0.116	thickness gap1	Length
hgpr2	= hgap2-2*t6250	0.132666666666667	thickness gap2	Length
hgpr3	= hgap3-2*t6250	0.674666666666667	thickness gap3	Length
w	= 0.4/3	0.133333333333333	width mic	Length
dx	= 9.31/3	3.10333333333333	dim grd plane	Length
dy	= dx	3.10333333333333		Length
h	= 2/3	0.666666666666667	ground plane gap	Length
dAdl	= 1.862/3	0.620666666666667	dim patch	Length
wAdl1	= 0.19/3	6.33333333333333e-02	dim patch slab1	Length
wAdl2	= 0.2/3	6.66666666666667e-02	dim patch slab2	Length
wAdl3	= 0.4/3	0.133333333333333	dim patch slab3	Length
hgap1	= 0.424/3	0.141333333333333	gap slab1	Length
hgap2	= 0.474/3	0.158	gap slab2	Length
hgap3	= 2.1/3	0.7	gap slab3	Length
dz1	= 0.127/3	4.23333333333333e-02	inter layer dist slab1	Length
dz2	= 0.33/3	0.11	inter layer dist slab2	Length
dz3	= 2/3	0.666666666666667	inter layer dist slab3	Length
t	= 0.254/3	8.46666666666667e-02	height of mic feed	Length
lc	= 2/3	0.666666666666667	dim capa	Length
ri	= 0.55/2/3	9.16666666666667e-02	inner radius (pin)	Length
xpos	= 2/3	0.666666666666667	coax position	Length
ro	= 0.91/3	0.303333333333333	outer radius	Length
l	= 3.8/3	1.26666666666667	length mic	Length
r	= 0.38/3	0.126666666666667	radius cover of mic	Length
rc	= 0.35/2/3	5.83333333333333e-02	radius core	Length
xfed	= 1.18/3	0.393333333333333	position 2nd core	Length
tx	= 2*0.35/3	0.233333333333333	translation of cores	Length
lslot	= 1.4/3	0.466666666666667	width slot	Length
L_slot	= 2.3/3	0.766666666666667	length	Length
L_tri	= 2.1/3	0.7	triangular cut	Length
red	= 133/100/3	0.443333333333333	middle slot	Length
Lx	= 1/3	0.333333333333333	dimension capa	Length
ty	= 2/3	0.666666666666667		Length
edg	= tx/2	0.116666666666667		Length
gap1	= 0.655/3	0.218333333333333	dielec transf	Length
y1	= 3/3	1	dielec transf	Length
x1	= 3/3	1	dielec transf	Length
gap2	= 2/3	0.666666666666667	dielec transf	Length
y2	= 3/3	1	dielec transf	Length
x2	= 3/3	1	dielec transf	Length
ty3	= 0.3/3	0.1	allign inside dielec	Length

Figure 43: Dimensions of the 26-39 GHz antenna

6.1. The infinite model

The infinite model is first considered in order to check the behaviour with respect to the predictions and the prototype.
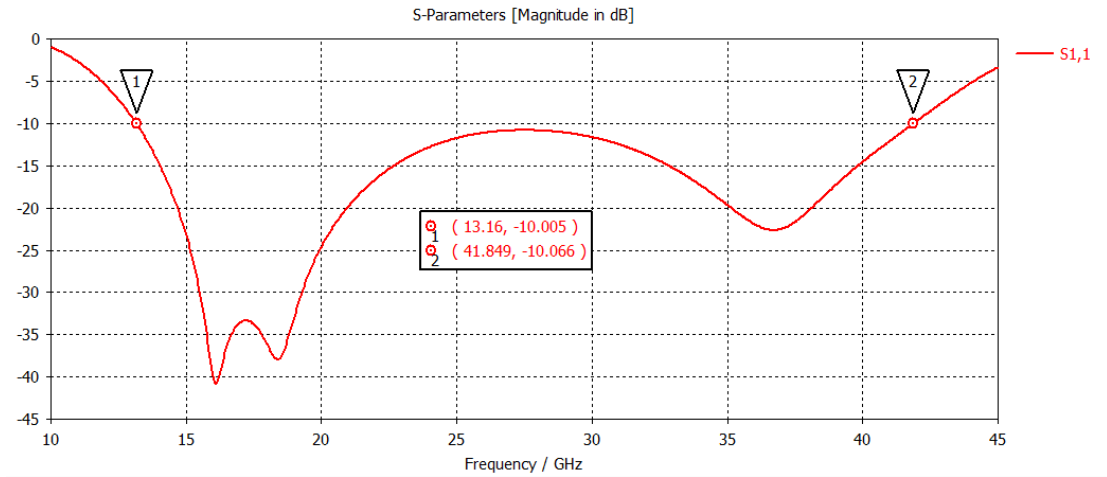
Figure 44: Reflection coefficient of the bi-band antenna in the infinite model

As predicted, the return loss is under -10dB between **13.16 GHz** and **41.849 GHz**, giving a bandwidth of **28.689 GHz.**

It should also be mentioned that some parameters had to be re-optimized to deal with the new antenna constraints, it is the case of the feeding capacitor ($l_c \times l_x = 2mm \times 1mm$).

The VSWR is also plotted :

Figure 45: VSWR of the dual band antenna in the infinite model

Under VSWR<2, the bandwidth realized is **BW=42.06-13.074=28.986GHz.**

At the end of this section, it can be confirmed that in infinite array configuration, the wideband performance of the prototype is observed for the dual band antenna as well.
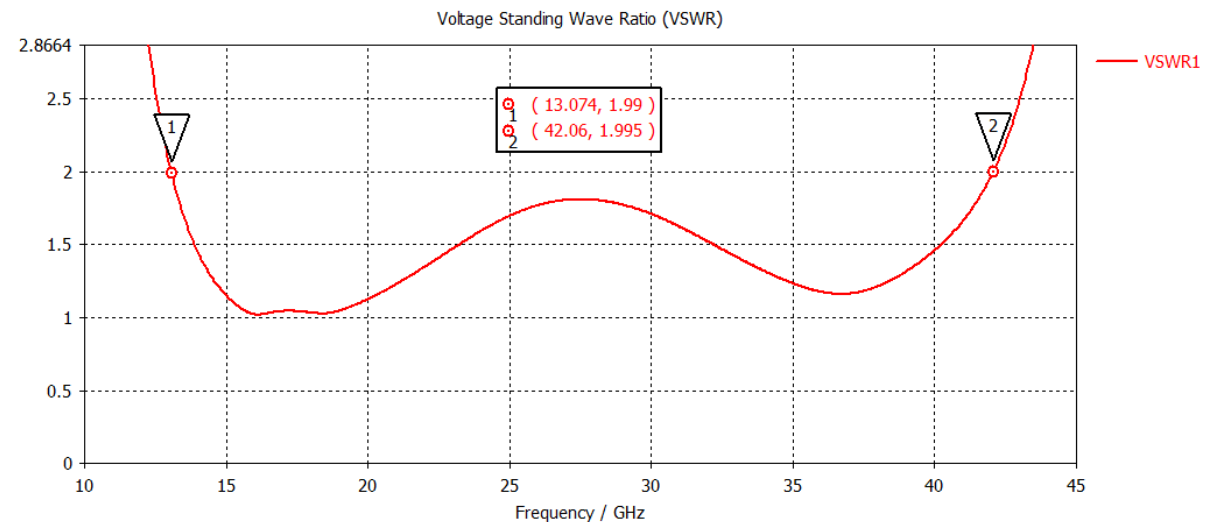
6.2. Metallic Walls

In practice, the infinite model is not realistic and unrealizable. A realistic one would be a finite array approach. In the next section we will detail this approach but before performing this task, we have to anticipate an eventual issue related to this configuration. Since in finite array, several antennas are placed close to each other, their radiation will induce huge coupling between them. To reduce the coupling, we decide to place metallic walls along the edges so that the antennas placed orthogonally to the slots have small mutual coupling.

The wall consists in a row of ten small PEC cylinders of radius **rc,** length **h** and spaced by *tx* (reported in figure 43). The cylinders are separated into two sets of five cylinders so that considering the feeding network we almost have a continue wall. The continue wall ensure that we have few waves escaping.
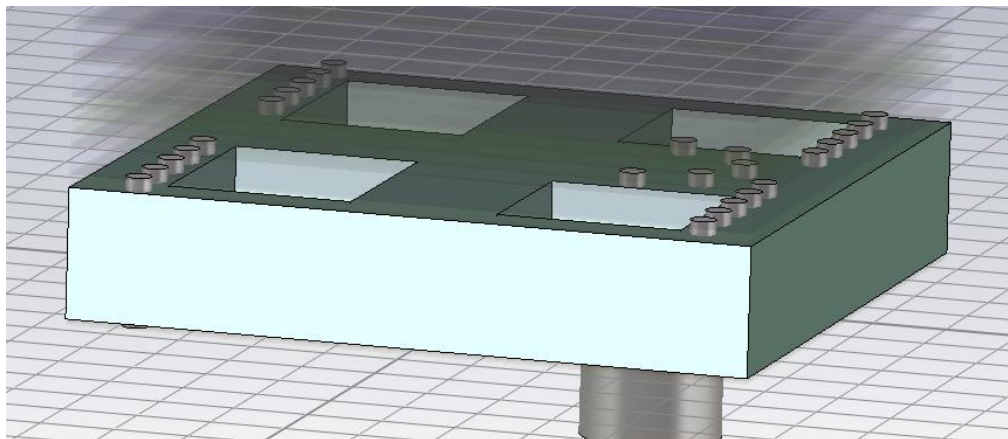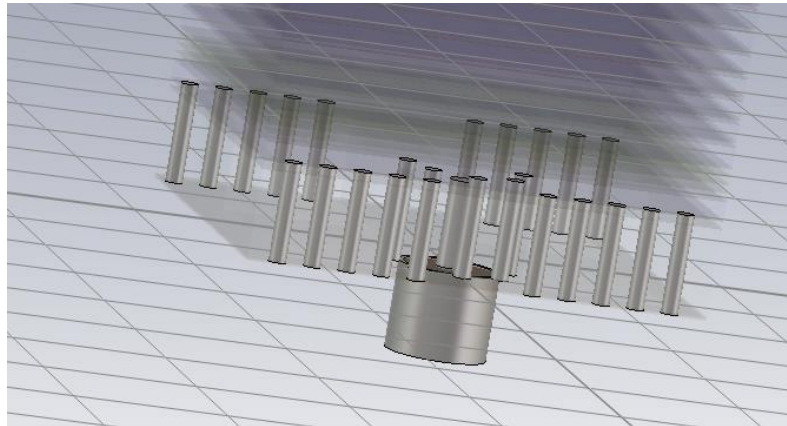

Figure 46: Metallic walls cancelling undesired coupling on the edges

6.3. Phased Array Antenna

A phased array is a set of two or more antennas. The signals from the antennas are combined for purpose of achieving improved performance with respect to a single antenna. Array antennas are used for many purposes like increasing the overall gain or directivity, steer the array so that it is most sensitive in a particular direction. These advantages are suitable for our antenna designed since 5G will require antennas able to transmit or received huge data in a particular direction at once to satisfy users.

6.3.1.   5x5 Array

The choice of a 25-elements array comes from different reasons like the size of the array, edges effect, feasibility. In a small array the edges effect will be considerable on the antennas while an important array size will be difficult to simulate with our logistics tool. A 5x5 array is then a reasonable choice.
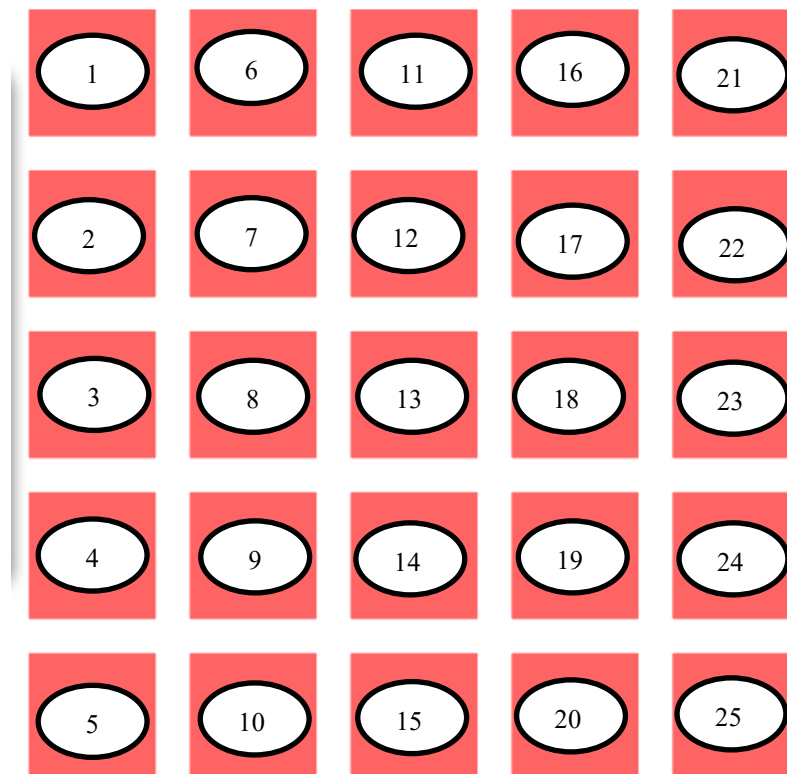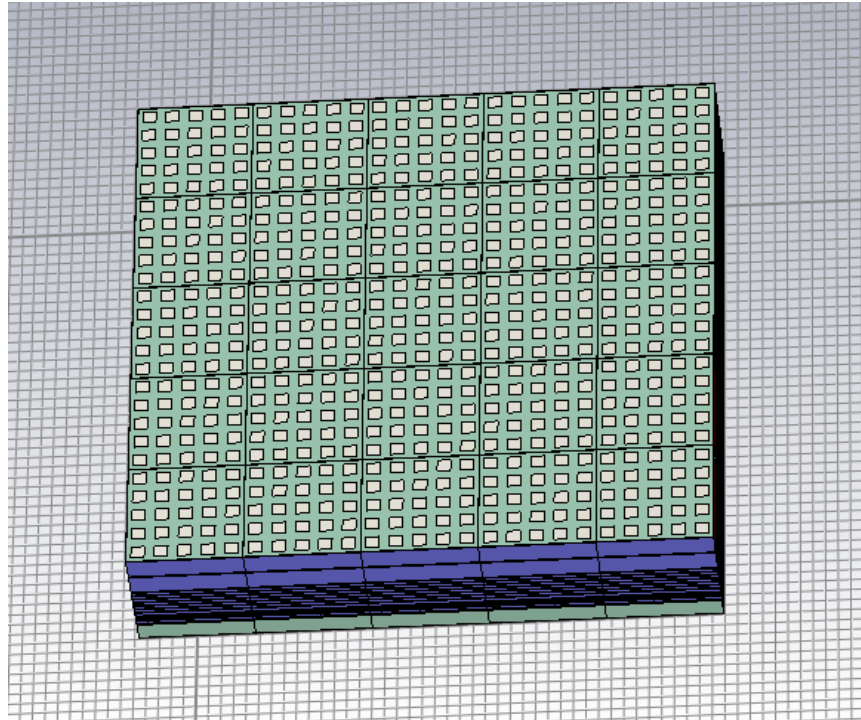
Figure 47: 5x5 Array setup

Figure 48: 3D view of the 5x5 array

The array is constructed by making copies of the unit cell the number of times required by the array. In this way, the simulation is run with open add space boundaries and simultaneous ports. After running the simulation, we get in the 1D results, the S-parameters of the array: the reflection coefficients and the transmission coefficients of all ports and the radiation pattern of each single antenna can be observed in the farfield results.

The global performances of the array are obtained only after using the tool " combine results " of CST. This task is done by applying the following steps :

Select the farfield folder → go to post-processing tab → combine results → set voltage at 1 for all ports → combine.

The active S-parameters appear now in S-parameters of the 1D results and we can analyse the performance of each antenna taking into account the presence of the neighbouring. The active S-parameter is the return loss when the mutual coupling with other antennas is taken into account.

In the following, we will analyse the active S-parameters obtained for each element of the array and conclude on its efficiency.
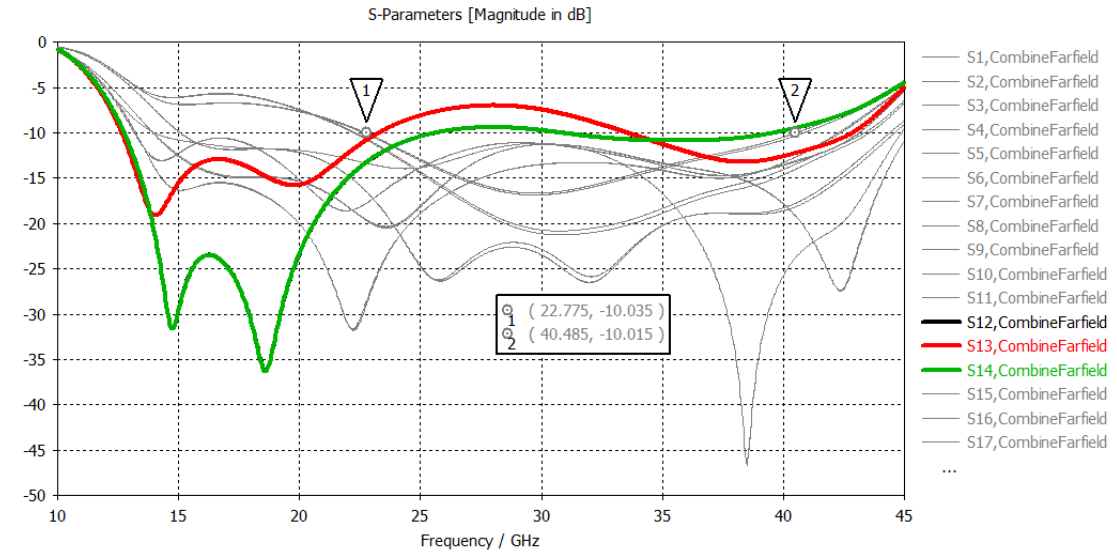
Figure 49: Active S-parameters of the 25-elements array

All the antennas are well matched ($S_{ii} < -10\,dB$) between **22.775 GHz** and **40.485 GHz** (corresponding to a bandwidth of **BW=17.71 GHz**) except the three antennas 12,13 and 14 which are the most centered antennas of the array. Moreover, the three antennas mentioned are well matched in the 39 GHz band while the high mutual coupling between them degrades their matching in the 26 GHz band. This is highlighted through the following curve :
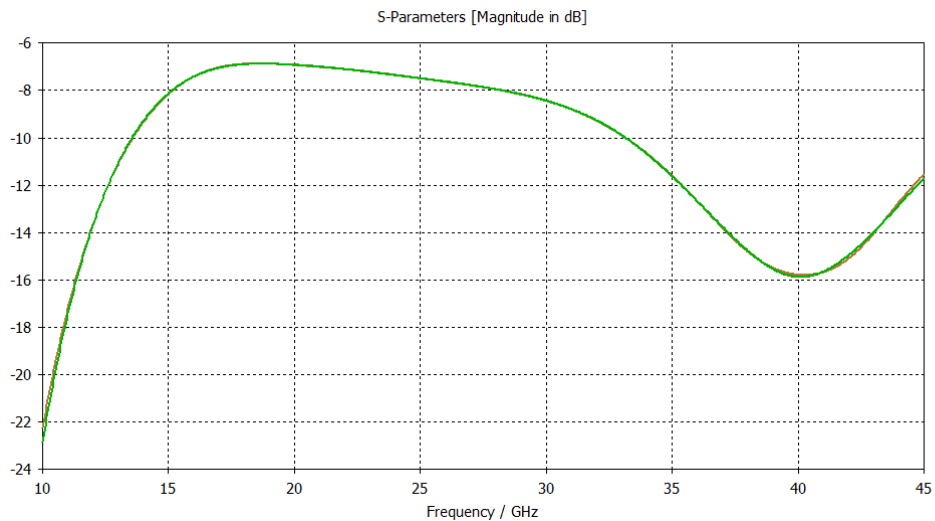
Figure 50: Mutual coupling between antenna 12, 13 and 14

Indeed, the coupling between antenna 12, 13 and 14 is important in the 26GHz band and negligible in the 39 GHz band.

55
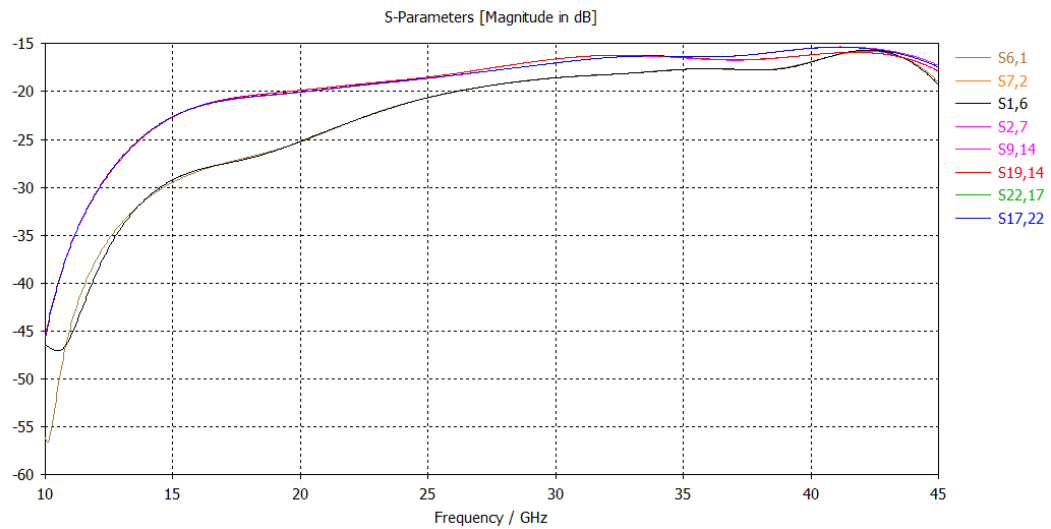
Figure 51: Mutual coupling between (1,6) ,(2,7),(9,14) and (17,22)

From the curves of figure 51 above, it is clearly visible that the coupling between horizontal antennas is very low thanks to the metallic walls.

Before approaching a solution to fix the matching of the three centered antennas, the farfield performances of the 5x5 array is highlighted below:
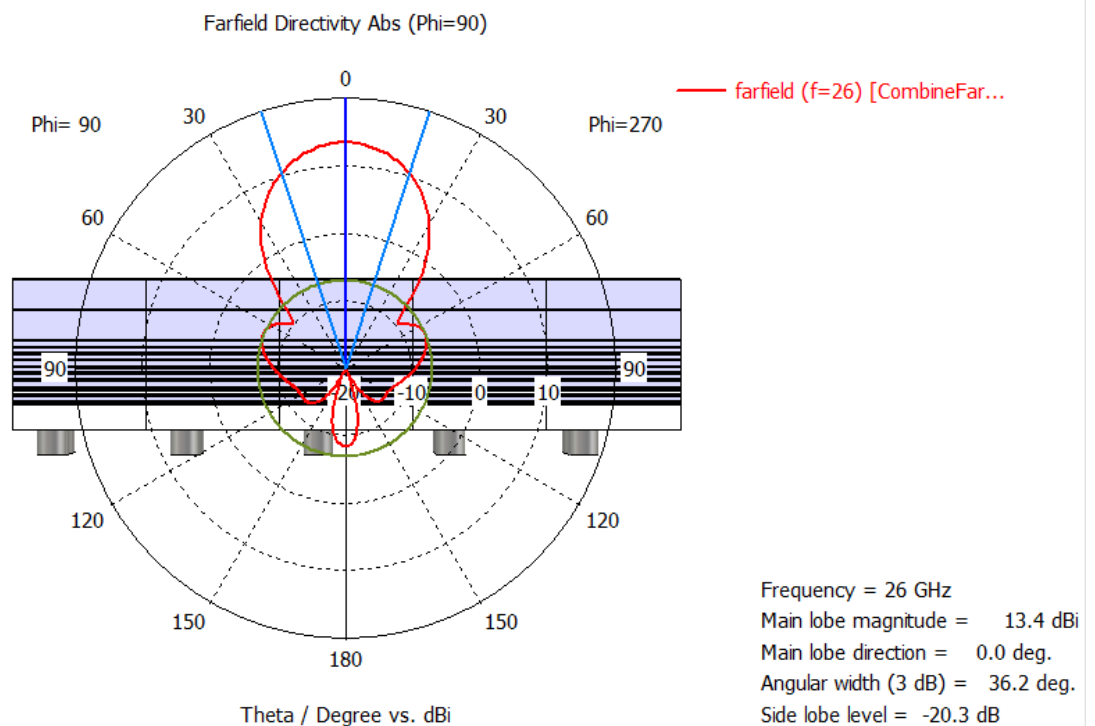
Figure 52: Farfield directivity of the 5x5 array at 26 GHz in polar plot

56
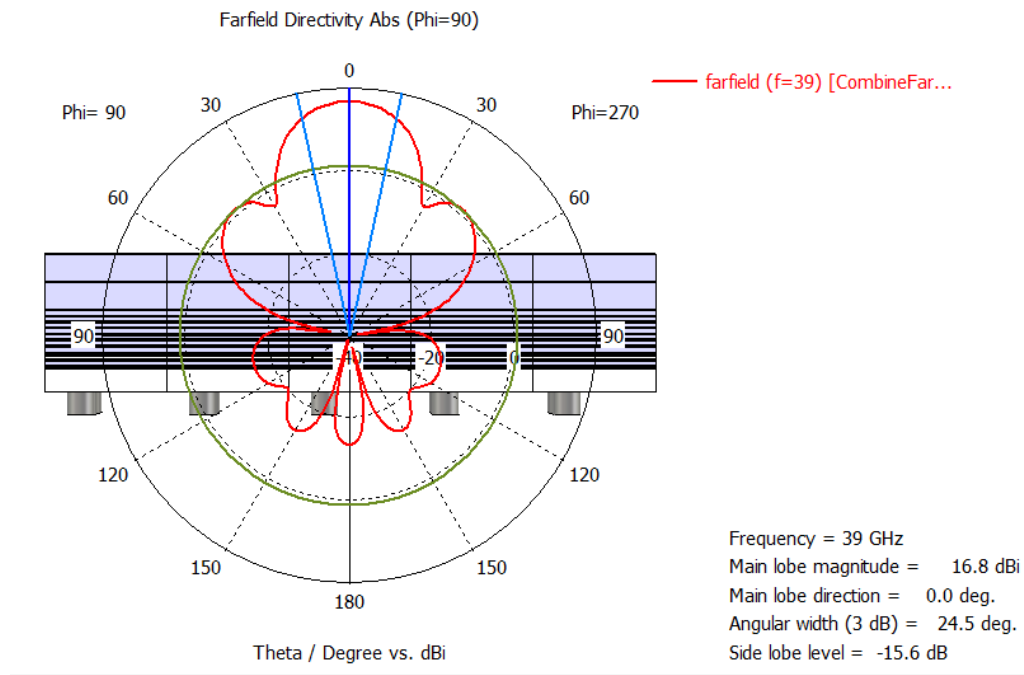
Figure 53: Farfield directivity of the 5x5 array at 39 GHz in polar plot

	Directivity [dBi]	Realized Gain [dB]	Total efficiency[dB]	Total efficiency [%]
26 GHz	13.40	13.17	-0.2328	94.78
39 GHz	16.79	16.55	-0.2381	94.67

Table 7: Farfield Performances of the 5x5 array

The global performance of the array is better compared to the single antenna. Besides, the performances improve with the frequency (directivity, gain) and the total efficiency remains good.

Now, to deal with the mutual coupling of the three centered antennas, the solution provided is to use a larger array so that the coupling of the centered elements is reduced by the added elements.

6.3.2.   7x7 Array

A 7x7 array is a good choice to the trade-off between the logistical tool and the issue related to the coupling of the centered antennas.
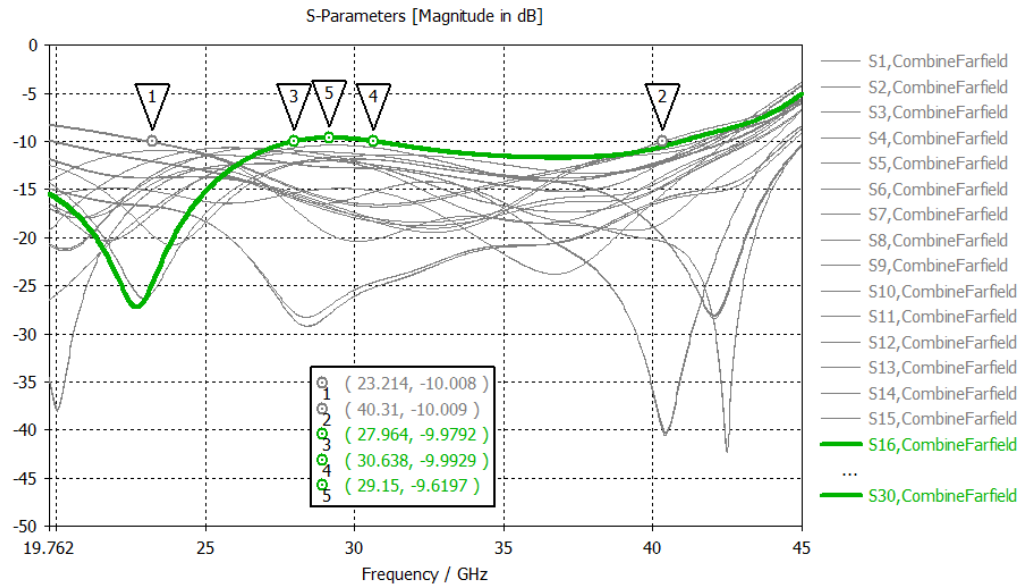
Figure 54: Active S-parameters of the 49-elements array

The active reflection coefficient of almost all the antennas is under **-10 dB** from **23.214 GHz** to **40.31 GHz,** resulting in a bandwidth of **BW=17.096 GHz**. The curves of **16,20,30** and **34** are merged on figure 54 because of symmetry and their curve is slightly above -10 dB from **27.964** to **30.638 GHz** but the pic value never exceeds **-9.61 dB.** Therefore, the assumption of all active S-parameters under -10 dB from **23.3** to **40.3** is an objective and realistic decision.
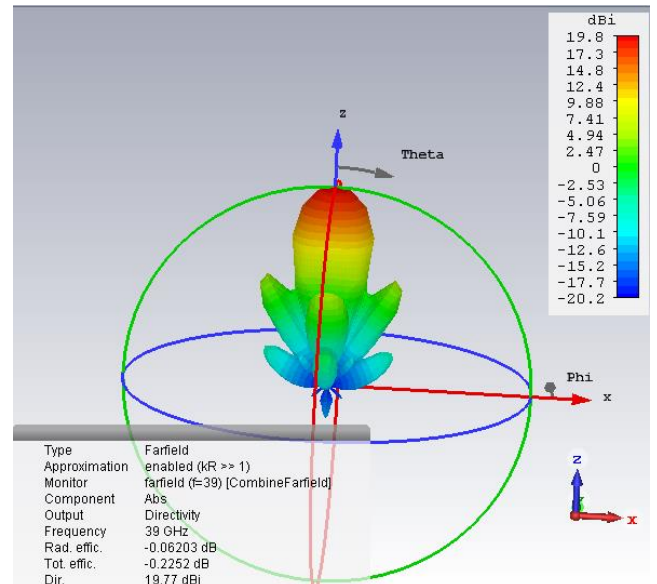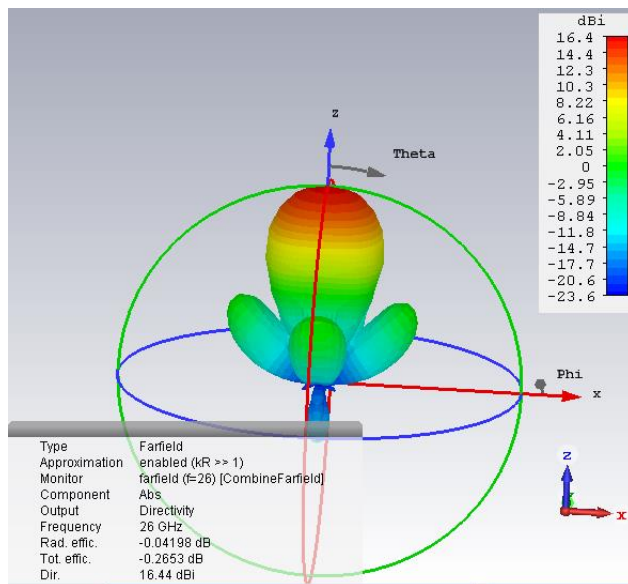
Figure 55: 3D radiation pattern of the 7x7 array at 26 and 39 GHz
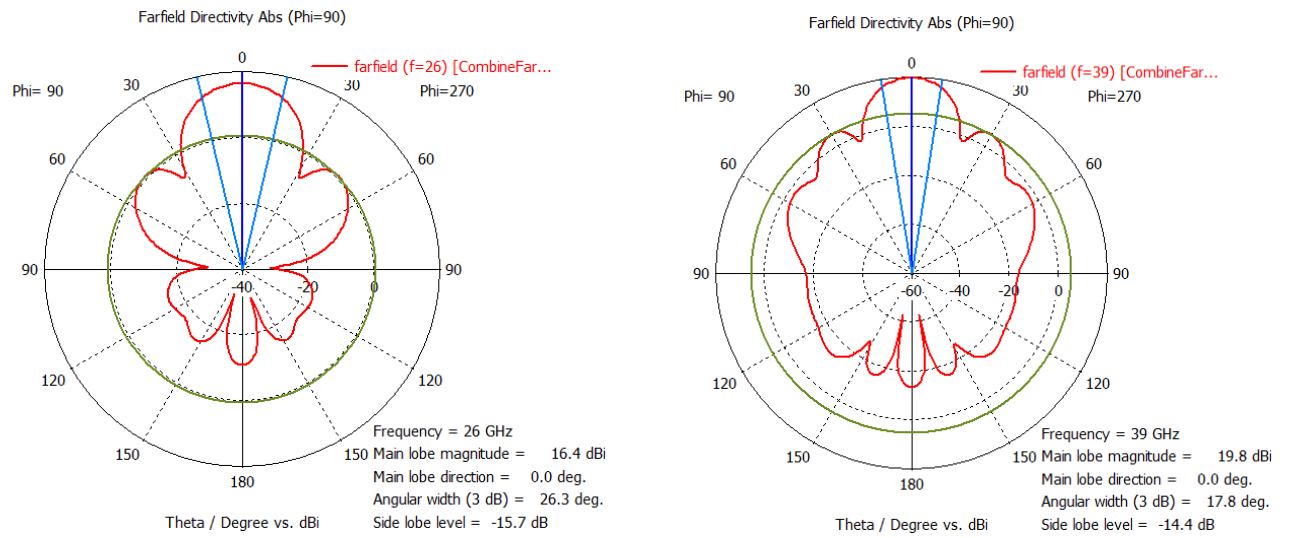
Figure 56: Farfield directivity of the 49-elements array at 26 and 39 GHz in polar plot

Regarding the results obtained in figure 55 and 56, one may say that the beam becomes more and more narrow with the size of the array and also with the frequencies. This is further confirmed by the following table showing an overview of the farfield results of the 7x7 array :

	Directivity [dBi]	Realized Gain [dB]	Total efficiency[dB]	Total efficiency [%]
26 GHz	16.44	16.17	-0.2653	94.07
39 GHz	19.77	19.54	-0.2252	94.95

Table 8: Summary of the farfield results of the 7x7 array

Basically, in the 49-elements array, we obtain higher directivity and gain compared to the 25-elements while keeping an efficiency of **94%** and all the active reflection coefficients under -10 dB, thus having a good matching on the 26-39 GHz dual band. Furthermore, the side lobes level (SLL) remains low.

59

7. Conclusion

This research aimed to design an antenna working in the 26-39 GHz bands of future ultra-fast 5G systems. Based on a first prototype of high frequency antenna working in the 6-15 GHz bands, a 7x7 wideband connected arrays of slots loaded with artificial dielectrics has been designed. This antenna has shown good performances in terms of matching, directivity and gain while maintaining a high efficiency.

During this internship at Orange labs, I was able to learn a lot in line with the training I took at Politecnico di Torino and ENSIL-ENSCI. The contributions I have drawn from my work experience are divided into two main parts : skills acquired and working independently in times of global health crisis. Despite the difficulties encountered, I can say that most of the assigned missions have been completed. I was really immersed in the heart of the business. This work experience was also an opportunity to discover new knowledge and deepen my skills. I definitely keep an excellent memory of the internship which is now a rewarding and encouraging professional experience for my future.

Finally, I would like to express my satisfaction at having worked in a pleasant environment with good material conditions.

8. Perspectives

The very last part of the project is to work on the steering capabilities of the antenna. The array must keep good matching on the two bands while providing less or more higher angle of steering in the E and H plane. The first goal is to reach a steering angle of 45° and try to improve if possible. This task will be completed during the remaining days of the internship.

Once this work achieved, a prototype will be manufactured and tested in the anechoic chamber.

9. **References**

[1] W. H. Syed, D. Cavallo, H. Thippur Shivamurthy, and A. Neto, " Wideband, Wide-scan planar array of connected slots loaded with artificial dielectric superstrates," *IEEE Trans. Antennas Propag.,* Vol 64, no. 2 Feb 2016.

[2] D. Cavallo, W. H. Syed and A. Neto, "Closed-form analysis of artificial dielectrics layers-Part I: Properties of a single layer under plane-wave incidence," *IEEE Trans. Antennas Propag.,* Vol 62, no. 12, pp. 6256-6264, Dec. 2014.

[3] D. Cavallo, W. H. Syed and A. Neto, "Closed-form analysis of artificial dielectrics layers-Part II: Extension to multiple layers and arbitrary illuminations," *IEEE Trans. Antennas Propag.,* Vol 62, no. 12, pp. 6265-6273, Dec 2014.

[4] R. J. Bolt, D. Cavallo, G. Gerini, D. Deurloo, R. Grooters, A. Neto and G. Toso, " Characterization of a dual-polarized connected dipole array for Ku-band mobile terminals," *IEEE Trans. Antennas Propag.,* Vol 64, no. 2, Feb. 2016.

[5] A. Neto, D. Cavallo, G. Gerini and G. Toso, " Scanning performances of wideband connected arrays in the presence of a backing reflector," ," *IEEE Trans. Antennas Propag.,* Vol 57, no. 10, Oct. 2009.

[6] D. Cavallo, W. H. Syed and A. Neto, " Connected-slot array with artificial dielectrics: a 6 to 15 GHz dual-pol wide-scan prototype," *IEEE Trans. Antennas Propag.,* Vol 66, no. 6, Jun. 2018.

[7] A. Neto, D. Cavallo and G. Gerini," Finiteness effects in wideband connected arrays: analytical models to highlight the effects of the loading impedances," Eucap 2011-Convened papers.

[8] A. Neto, D. Cavallo and G. Gerini, "Edge-born waves in connected arrays: A finite x infinite analytical representation," *IEEE Trans. Antennas Propag.,* Vol 59, no. 10, Oct. 2011.

[9] D. Cavallo, W. H. Syed and A. Neto, " Equivalent transmission line models for the analysis of edge effects in finite connected and tightly coupled arrays," *IEEE Trans. Antennas Propag.,* Vol 65, no. 4, Oct. 2017.

[10] W. H. Syed and A. Neto, "Front-to-back ratio enhancement of planar printed antennas by means of artificial dielectric layers," *IEEE Trans. Antennas Propag.,* Vol 61, no. 11, Nov. 2013.

[11] D. Cavallo, W. H. Syed and A. Neto, " A 5:1 connected slot array loaded with artificial dielectric layers," *invited paper*.

[12] Prof. Ladislau Matekovits, Ph.D. ,"Lecture: REMS MWS introduction," *Department of Electronics and Telecommunications, Politecnico di torino,* March 2019.

[13] Mario Orefice, " Antenna design notes Part I," *Department of Electronics and Telecommunications, Politecnico di torino,* 2013.

[14] www.antenna-theory.com

10. Appendices

10.1. Appendix A

```
%% Paper:Closed-Form Analysis of ADL--Part 1 and Part 2; Dec 2014
close all;
clc

%%
% theta,phi : angles towards which the arrray is pointing
m=1001; % number of frequency points
thetad =45;% angle in degree %linspace(0,pi,n); % angle between the z-axis and the vector
from the origin to the point
phid   = 0.0001;% angle in degree %linspace(0,2*pi,n); % angle between the x-axis and the
projection of the point onto the x-y plane
theta=pi*thetad/180; % angle in radian
phi=pi*phid/180; % angle in radian
fo=15e9; % maximum frequency of investigation [GHz]
f=linspace(0.3*fo,fo,m); %frequency range
c=3e8; % speed of the light
lambda_0=1000.*c/fo; % wavelength at the maximum frequency of investigation fo
lambda=1000.*c./f;

%% parameters
ko=(2*pi)./lambda;% propagation constant in free space %% sweep on Freq range
kxo=ko.*sin(theta).*cos(phi);
kyo=ko.*sin(theta).*sin(phi);
dx=0.15*lambda_0; % period along x

% D(kx): transverse connected array Green's function
dy=0.15*lambda_0; % period along y
dz=0.012*lambda_0;%inter(layer dist
ws=0.02*lambda_0; % width of slot
psi=377;% free-space impedance [ohm]

%% Calculation of Bs infinite / Bs semi infinite
syms my ;
app1=5;
b=10; % upper and lower bound for Bs_inf
%% Calculation of Bs / Single layer
ft=1-(sin(theta)^2)/2; %transformation factor
kym_bs=(2*pi.*my)./dy; %single layer
d3=abs(kym_bs);%coeff of Bs /single layer
c3=abs(sinc((kym_bs.*ws)./2)).^2;%coeff of Bs
a3=(2*ko)./psi; %coeff of Bs
g3=(a3.*c3)./d3;
Bs= vpa(symsum(g3,my,1,b)+symsum(g3,my,1,b),app1);

%% Reactance of a single layer
```

```matlab
Zlayer_TM=-1i./(Bs);
Zlayer_TE=-1i./(Bs.*ft);

%% Plotting
figure(1)
plot(f,imag(Zlayer_TM),'g-',f,imag(Zlayer_TE),'m-');
grid on;
xlabel('Frequency');
ylabel('Im(Z_{layer}) [\Omega]');
legend('TM','TE');
title(" Equivalence capacitance of a single layer for TE and TM incidence");
```

10.2. Appendix B

```matlab
%% Paper:Closed-Form Analysis of ADL--Part 1 and Part 2; Dec 2014
%%
close all;
clc
% theta,phi : angles towards which the arrray is pointing
n=3; % number of scanning angles
m=1001; % number of frequency points
thetad =45;% angle in degree %linspace(0,pi,n); % angle between the z-axis and the vector
from the origin to the point
phid   = 0.0001;% angle in degree %linspace(0,2*pi,n); % angle between the x-axis and the
projection of the point onto the x-y plane
theta=pi*thetad/180; % angle in radian
phi=pi*phid/180; % angle in radian
fo=15e9; % maximum frequency of investigation [GHz]
f=linspace(0.3*fo,fo,m); %frequency range
c=3e8; % speed of the light
lambda_0=c/fo; % wavelength at the maximum frequency of investigation fo
lambda=c./f;

%% parameters
ko=(2*pi)./lambda;% propagation constant in free space %% sweep on Freq range
kxo=ko.*sin(theta).*cos(phi);
kyo=ko.*sin(theta).*sin(phi);
dx=0.15*lambda_0; % period along x

% D(kx): transverse connected array Green's function
dy=0.15*lambda_0; % period along y
dz=0.012*lambda_0;%inter(layer dist
ws=0.03*lambda_0; % width of slot
psi=377;% free-space impedance [ohm]

%% Calculation of Bs infinite / Bs semi infinite
```

```
syms my ;
b=10; % upper and lower bound for Bs_inf
a=10; % upper and lower bound for Bs_semi inf
app1=5;%approximation of Bs_inf
app2=5;%approximation of Bs_semi_inf
kym=(2*pi.*my)./dy; %kyo-((2*pi.*my)./dy);
kzm=-1i*abs(kym); %inter-layer distance
c=abs(sinc((kym.*ws)./2)).^2;%coeff of Bs
d=abs(kym);%coeff of Bs
%Bs_inf
a1=(2*ko.*1i)./psi; %coeff of Bs_inf
h1=tan((kzm.*dz)./2);%coeff of Bs_inf
g1=(a1.*c.*h1)./d; %function of Bs_inf
Bs_inf= vpa(symsum(g1,my,-a,-1)+symsum(g1,my,1,a),app1);
%Bs_semi_inf
a2=ko./psi;%coeff of Bs_semi inf
h2=1+1i*tan((kzm.*dz)./2);%coeff of Bs_inf
g2=(a2.*c.*h2)./d; %function of Bs_semi_inf
Bs_semi_inf= vpa(symsum(g2,my,-a,-1)+symsum(g2,my,1,a),app2);
%Displaying
% disp(Bs_inf);
% disp(Bs_semi_inf);

%% convergence of Bs_inf
% r1=0;
% r=Bs_inf;
% diff_1=abs(r-r1);
% epsilon=1e-5;% precision
%  while diff_1 >= epsilon
%    r1=r;
%    b=b+1;
%    r= vpa(symsum(g1,my,-b,-1)+symsum(g1,my,1,b),app1);
%    diff_1=abs(r-r1);
% end
% disp(b);
% disp(r);
% %% convergence of Bs_semi inf
% r2=0;
% r3=Bs_semi_inf;
% diff_2=abs(r3-r2);
% epsilon2=1e-5;% precision
%  while diff_2 >= epsilon2
%    r2=r3;
%    a=a+1;
%    r3= vpa(symsum(g2,my,-a,-1)+symsum(g2,my,1,a),app2);
%    diff_2=abs(r3-r2);
% end
% disp(a);
% disp(r3);

%% Reactance of layer embedded in a periodic multilayer environment
ft=1-(sin(theta)^2)/2; %transformation factor
```

```matlab
Zinf_TM=-1i./(Bs_inf);
Zinf_TE=-1i./(Bs_inf.*ft);
% disp(Zinf_TM);
% disp(Zinf_TE);

%% Calculation of Bs / Single layer
kym_bs=(2*pi.*my)./dy; %single layer
d3=abs(kym_bs);%coeff of Bs /single layer
c3=abs(sinc((kym_bs.*ws)./2)).^2;%coeff of Bs
a3=(2*ko)./psi; %coeff of Bs
g3=(a3.*c3)./d3;
Bs= vpa(symsum(g3,my,-b,-1)+symsum(g3,my,1,b),app1);

%% Reactance of a single layer
Zlayer_TM=-1i./(Bs);
Zlayer_TE=-1i./(Bs.*ft);

%% Plotting
plot(f,imag(Zinf_TM),'b-',f,imag(Zinf_TE),'r-',f,imag(Zlayer_TM),'g-',f,imag(Zlayer_TE),'m-');
grid on;
xlabel('Frequency');
ylabel('Im(Z_{layer}) [\Omega]');
legend('TM Multi layers','TE Multi layers','TM Single layer','TE Single layer')
title("Single layer vs layer embedded in a cascade of layers");
```